Optimal configuration of a wind-photovoltaic-hydrogen-gas-electric vehicles integrated energy system considering multiple uncertainties and carbon reduction

Gang Zhu, Yan Gao*, Hao Sun

School of Management, University of Shanghai for Science and Technology, Shanghai 200093, China

Abstract

Coupling renewable energy, electric vehicle and hydrogen storage is an effective way for integrated energy systems (IES) to move toward a low-carbon approach. The uncertainties of wind power, PV power and load demand are considered, meanwhile, a ladder-type carbon trading mechanism is designed, and the model is transformed into a deterministic Mixed-integer linear programming (MILP), while the reliability of spinning reserve power is measured by a proper confidence level. Meanwhile, the objective function is constructed based on the optimization strategy of deviation preference, and two objectives are introduced to optimize the annual comprehensive cost and annual carbon emission. The problem is transformed into a MILP and the optimization of the capacity configuration of this IES is performed. The results show that the IES has advantages in economic and environmental performance. The IES has significant advantages in carbon dioxide emission reduction (CDER); meanwhile, EVs show advantages in CDER and charging cost compared to those in the non-IES. Carbon dioxide emissions in IES are only one-fifth of those of conventional distribution system and the CDER effect is noticeable. Moreover, EV charging cost in the IES is relatively lower, while the CDER effect is an order of magnitude better than that of non-IES.

Keywords: Integrated energy system; Uncertainty; Deviation preference; Capacity configuration; Carbon dioxide emission reduction

* Corresponding author.
E-mail address: gaoyan@usst.edu.cn (Y. Gao)
doi:

Nomenclature

Abbreviations

IES	Integrated energy system
CDS	Conventional distribution system
REPG	Renewable energy power generation
HESS	Hydrogen Energy Storage System
CCHP	Combined cooling heating and power
AUES	Auxiliary equipment system
CDE	Carbon dioxide emission
CDER	Carbon dioxide emission reduction
TOU	Time-of-use
EV	Electric Vehicle
EVO	Electric Vehicle Owner
EVG	Electric Vehicle Group
ACC	Annual comprehensive cost
ACE	Annual carbon emission
MILP	Mixed-integer linear programming
PSO	Particle swarm optimization
LC	Life cycle
EH	Energy hub
MC	Monte Carlo
PV	Photovoltaic Panel
WT	Wind turbine
WHB	Waste heat boiler
AC	Absorption chiller
ELZ	Electrolyzer
HST	Hydrogen storage tank
FC	Fuel cell
EC	Electric cooler
CGT	Conventional gas turbine
GB	Gas boiler
PGST	Power-to-gas-to-storage tank
SOC	State of charge
DEP	Dumped energy proportion
LPSP	Loss of power supply probability
CCT	Carbon capture technology
HFCV	Hydrogen fuel-cell vehicle
V2G	Vehicle to grid
DST	Discretized step transformation
CCP	Chance-constrained programming
SOT	Sequence operation theory

Parameters

p_{vally}	Electrical price in the valley period
p_{peak}	Electrical price in the peak period
η	The proportion of EVOs affected by demand response
N	The number of EVOs
D_{EV}	The private EVs daily mileage
t_c	Charging duration time
P_i	The charging power of the i-th EV
P_{lk}	The charging power demand at the k-th hour of the l-th day
N_{pv}	The number of PV panels in the PV array
P_{rpv}	The rated power of PV panels in a standard environment
f_{pv}	The attenuation coefficient of PV
$R_a(t)$	Actual light intensity at time t
R_S	Light intensity in the standard environment
k	Power temperature coefficient
$T_a(t)$	The actual temperature of PV panel at time t
T_S	Standard ambient temperature
T_{ae}(t)	Actual ambient temperature
P_{wt}^{rated}	The rated power of WT
V_{in}	Cut-in wind speed
V_{out}	Cut-out wind speed
V_r	Rated wind speed
$V(t)$	System actual wind speed at time t
Q_{gas}	The consumption of natural gas
Q_{nb}	The heating load supplied by the GB
P_{gt}	The output power of GT
Q_{gb}	The heat load provided by the GB
β_1	The power generation efficiency of GT
β_2	The heating efficiency of GB
δ	The minimum heat of combustion value of natural gas
ε	The heat loss coefficient of GT
H_{whb}	The waste heat used by WHB
H_{ac}	The waste heat used by AC
Q_{whb}	The heat load supplied by WHB
Q_{ac}	The heat load supplied by AC
Q_{eb}	The heat load supplied by EB
γ_{ac}	The cooling performance coefficient of AC
γ_{whb}	The conversion efficiency of WHB
γ_{eb}	The conversion efficiency of EB
$P_{sum}(t)$	The total power generation in time slot t
$P_{TE}(t)$	The electric power in time slot t
τ_1	The efficiency of the converter
τ_2	The efficiency of the electrolyzer unit
τ_3	The efficiency of fuel cell
φ_1	CO_2 emitted by burning $1m^3$ of natural gas

1. Introduction

1.1. Background and motivation

Economic development is accompanied by an increase in energy demand and carbon emissions. Net CO_2 emissions from human activities must approach zero to stabilize the global average temperature [1]. Energy-related CO_2 emissions (CDEs) account for two-thirds of global greenhouse gas emissions, and energy consumption will increase by 44% from 2006 to 2030 [2]. Therefore, an energy transition is called for now to break the link between economic growth and rising greenhouse gas emissions. The ideal energy source must be affordable, accessible and sustainable [3], thus providing reliable, economical and environmentally friendly power is the focus of today's society. When the carbon dioxide concentration doubled, the global average temperature increased by 2.3 degrees [4], which provides a quantitative target for carbon dioxide emissions for humans to control rising temperatures [5]. IES has advantages in improving autonomic operation and reducing carbon emissions [6]. Decarbonization by shifting to renewable energy power generation (REPG) is an essential solution to address the energy crisis in the transition. How to coordinate and optimize the use of various energy sources is a subject of planning, design and operation in the IES. Deploying REPG technologies is a promising effort that humans can make to reduce the dramatic impact of climate change on our lives. However, REPG is mostly intermittent and fluctuating, to overcome the uneven distribution and dynamic availability of REPG, supplemental generation or storage is needed to keep balance. As the REPG capacity connected to the grid increases, so does the need for energy storage to avoid curtailment to match non-concurrent demand. Indeed, there are important synergies between hydrogen and renewable energy, as hydrogen significantly increase the growth potential of the renewable energy market. The hydrogen energy storage system (HESS) is capable of storing energy on a large-scale, cross-seasonal and efficient way. The collaborative operation of the HESS effectively improves the utilization of REPG and meet the demand of various types of loads. Hydrogen storage will become more competitive when the demand for energy interaction increases in the long term [7]. Compared with other energy storage, HESS has the strengths of green and clean, high energy density, high utilization efficiency, convenient transportation, and high-volume storage [8], which is believed to be a promising candidate to lead to a new hydrogen economy [9]. The cost of hydrogen storage is at least an order of magnitude lower than the cost of electric storage in large-scale energy storage. HESS is used not only to store hydrogen but also to provide hydrogen for fuel cells (FCs) or chemical production [10]. Moreover, EVs are

becoming increasingly popular as the fuel prices increase and the policies support of government on EVs [11]. By absorbing the power generated by REPG into the HESS and unlocking the potential of REPG, the flexibility of the IES is improved.

The targets will be achieved by selecting suitable equipment types and configuration capacities to fully utilize the REPG, meet the energy needs of various loads, and reduce the annual comprehensive cost (ACC) and carbon dioxide emissions (CDEs).

1.2. Literature review

IES, consisting of REPG, CCHP, HESS and the auxiliary equipment system (AUES), has attracted many scholars. As for the optimization models, a multi-objective model for biomass IES was established to configure capacity to improve the comprehensive performance of energy, economy and environment [12]. The optimization of hybrid REPG was developed to meet the specific daily residential load situation in remote areas [13]. A bi-level optimal dispatch model for the community IES with an EV charging station in multi-stakeholder scenarios was proposed [14]. A machine learning based approach was proposed in renewable microgrids based on remote switching of tie and sectionalizing considering a reconfigurable structure [15]. A capacity configuration model of the biogas IES was constructed and the capacity of the Pareto curve for the construction of the rural IES was obtained [16]. Off-grid communities were constructed to meet both electricity and thermal load demands simultaneously [17]. A REPG model was developed to meet the electrical load demand of a large reverse osmosis desalination plant [18]. The economics of three grid-independent hybrid renewable energy systems, proposed for co-generated electricity and heat for small-scale loads, were scrutinized [19].

As for the optimization tools, a framework with deep coupling of electricity-gas networks was constructed, using a game-theoretic approach and a particle swarm optimization (PSO) algorithm to derive an energy dispatch strategy [20]. A ant lion optimizer was proposed to solve the problem of optimal sizing and placement of distributed generation in a distribution system [21]. A bi-level model approach was used for a coupled cogeneration multi-energy system and a correlation model was developed for configuration and operation optimization [22]. An operation strategy was designed to solve the optimal operation schedule of CCHP, the optimal maintenance schedule of gas engines and the optimal capacity configuration of CCHP [23]. An optimal planning framework considering

compressed air energy storage and sliding time window for electric-thermal integrated demand response (IDR) to optimize the system capacity configuration and energy management strategy was proposed [24]. An optimization model with coordinated optimization of PV-battery systems with PV arrays and batteries under smooth scenarios was proposed [25]. A multi-objective genetic algorithm in a CCHP system was constructed with objectives including primary energy saving, life cycle(LC) cost reduction, CDER, comprehensive evaluation index [26]. A heuristic optimization approach was proposed to make a transactive strategy in distribution networks for purposeful pricing of distributed energy resources [27]. Multi-Objective Particle-Swarm Optimization (MOPSO) algorithm was taken to analysis the benefits of the exergy, exergo-economic, and exergo-environmental result in a waste-to-energy power plant [28]. The optimal size was determined in a hybrid system comprising WT/PV/diesel generator/battery using Mixed Integer Nonlinear Programming (MINLP) method and GAMS [29].

On the demand side, there are studies on customer preferences, demand load and demand response. A stochastic optimization model considering the dynamic characteristics of the network and psychological preferences was proposed, focusing on the influence of consumers' psychological preference factors, the results showed that the psychological preferences have a great influence [30]. EV will be an essential demand load of an IES in the future. An optimal hybrid energy selection method was proposed for hybrid EVs that include an ultracapacitor and a fuel cell with a battery unit [31]. It was proposed to incorporate EV load into distributed energy systems and to adopt a two-stage collaborative optimization algorithm for capacity configuration and operation optimization of zero-energy community systems [32]. A two-stage optimization method was presented for a coupled capacity planning and operation problem in a regional integrated energy system [33]. On demand response (DR), an optimal planning model considering price-based DR and incentive-based DR was proposed to evaluate and validate the environmental and economic benefits of DR strategies in grid-connected IES [34]. The concept of DR was extended and a double objective operation optimization model considering IDR mechanism with electric and thermal loads, a multi-objective operation optimization model with the objectives of economic efficiency and integrated energy efficiency were proposed [35]. In addition, a bilevel programming model for multi-regional IES was developed by solving the real-time pricing to maximize social welfare [36]. A bi-level programming model for integrated energy was developed to maximize the utilities of the players by a fuzzy max-min approach [37]. Recent research on optimizing the capacity configuration of IESs is summarized in

Table 1.

Most previous studies have not adequately addressed the diversity of device types, lack IES coupling REPG with HESS considering multiple uncertainties, rarely considered both renewable energy and load uncertainty, spinning reserve, electric vehicles as flexible loads, and interaction with the external main grid. In our work, all these factors are considered.

1.3. Contributions

The main contributions are summarized below:

1) The IES is complex and realistic. HESS effectively solve the waste of REPG. CCHP supports various cooling and heating loads, while AUES ensures energy supply in certain periods to meet the demand of various

loads.

2) Multiple uncertainties are considered. In this IES, stochastic EV loads, intermittent REPG and fluctuating load demand are studied.

3) The economic and environmental performance is compared and evaluated. Meanwhile, the carbon emissions of IES and non-IES are compared, and the economic and environmental performance of the EVG is also evaluated.

4) Various scenarios are analyzed to show the effects on economy, environment and reliability, by setting the confidence level of the appropriate spinning reserve constraint, a trade-off between economy and reliability is achieved.

5) A ladder-type carbon trading mechanism is designed by constructing a piecewise linear function, meanwhile, carbon tax policy is analyzed.

2. Mathematical model

The structure of the constructed natural wind-PV-hydrogen-gas-EV IES is shown in Figure 1, which contains four main subsystems: REPG, HESS, CCHP and AUES. The energy flows include natural gas, hydrogen, electricity, thermal and cooling energy. Hydrogen is suitable for production in centralized facilities in remote areas, power parks, fuel stations, distributed facilities, rural areas and customers' sites. However, the high cost of hydrogen energy production is still one of the critical obstacles to its widespread application. Therefore, IES should be prioritized for the following industrial parks: (i) It contains various loads to facilitate nearby energy consumption; (ii) Rich wind and solar resources, available to develop REPG;(iii) Near the main roads and chemical plants, available for the transportation of hydrogen energy.

The industrial park's electrical load is supplied by PVs, WTs, GTs and FCs, while also meeting the stochastic charging needs of EVs; the thermal load is supplied by GBs and WHBs; ACs and ECs are assigned to supply the cold load. The hydrogen load is supplied from two sources: surplus power for hydrogen from electrolysis when there is an excess power supply and purchased hydrogen transported in long tube trailers. When FCs are discharged to the IES, the fuel comes from hydrogen produced by the electrolyzer or purchased hydrogen.

2.1. EVs load modeling

2.1.1. EVs charging model

Although the individual EV charging is random, it will show a specific distribution when a certain size of EVs is reached. The change in charging price has some influence on their charging behavior, some EVOs can adjust the

charging time by the electricity price under a time-of-use (TOU) pricing environment. The distribution function of the charging price of EVs is as follows:

$$f_p(t)=\begin{cases} p_{valley} & t_{start}\le t\le t_{end} \\ p_{peak} & \text{else} \end{cases} \tag{1}$$

where p_{vally} denotes the electricity price in the valley time and p_{peak} denotes the electricity price in the peak hour, t_{start} and t_{end} denotes the moment when the valley time starts and ends. Assumptions include: (i) EVOs tend to charge vehicles at low electricity prices. (ii) No unexpected events occurring to affect EVOs. (iii) Charging power is uniformly distributed in the range of [3.5,7]; battery capacity is uniformly distributed in the range of [60,70]; (iv) Price-based demand response (PBDR) scheme was designed in TOU prices environment. The proportion of EVOs who follow the PBDR is η ($0<\eta<1$) of the total EVOs during the valley hours; EVOs are divided into two parts, N (N_{PDR} plus N_{NPDR}) EVs: $N_{PDR}=N*\eta$, $N_{NPDR}=N*(1-\eta)$, where N_{PDR} denotes the numbers of EVOs affected by charging prices and N_{NPDR} represents those not affected.（v）The starting time not affected by PBDR obeys a normal distribution, while affected by PBDR obeys a uniform distribution. (vi) The charging process is simplified to constant power charging. The D_{EV} of private EVs daily trips approximately meets a lognormal distribution [38]. The starting time of charging t_s not affected by PBDR adopts piecewise normal distribution [39]. For EVOs affected by PBDR， the starting time of charging t_s^{PDR} is calculated as follows:

$$t_s^{PDR}=\begin{cases} t_{valley}^{start}+rand\times\left(t_{valley}^{end}-t_c\right) & 0\le t_c\le t_{valley}^{end}-t_{valley}^{start} \\ t_{valley}^{start} & \text{else} \end{cases} \tag{2}$$

where t_{valley}^{start} and t_{valley}^{end} denotes the starting and ending time of the valley price. Rand indicates a random number in the range of the interval range in [0,1]. The above equations show that when the power consumption time of EVOs is greater than the interval duration of the valley hours, EVOs choose to charge at t_{valley}^{start} ; when the EVOs charging time is less than the interval duration of the valley hours, the charging time is chosen randomly within the interval. The charging duration of a single EV $t_c=\dfrac{D_{EV}P_{pchk}}{100\delta_c P_c}$ [39] , where P_{pchk} is the electricity consumption per 100 km; P_c is the charging power; δ_c is the EV charging conversion efficiency. Thus, the total charging power per hour is

calculated. By simulating the charging behavior of each EV each day, we obtain:

$$\begin{cases} A_{lik}=1 & \text{if the EV } i \text{ is charging at hour } k \text{ of day } l \\ A_{lik}=0 & \text{if the EV } i \text{ is not charging at hour } k \text{ of day } l \end{cases} \tag{3}$$

where $1 \le l \le 365$; $1 \le i \le N$; $1 \le k \le 24$ and all are integers. Therefore, the EVs load is calculated below:

$$P_{lk}=\sum_{i=1}^{N} P_i A_{lik} \tag{4}$$

where P_i is the charging power of the i-th EV; P_{lk} is the charging power demand at the k-th hour of the l-th day.

2.1.2. Monte Carlo simulation of EVs charging

MC simulation is introduced to simulate the electricity demand of large-scale EVs and obtain the electricity demand of N EVs at each time slot of the day to derive a typical daily EV charging demand, EVO contains two parts: ηN denotes the numbers of EVs complying with the PBDR scheme and $(1-\eta)N$ denotes those of randomly EVs charging, η = 20%, and the two are independent. The specific simulation diagram is shown in Figure 2. By MC simulation, the EV load curve is derived at different η and N, as shown in

Figure 3. Sensitivity analysis of EV charging is shown in Figure 4.

2.2. Uncertainties modeling

The uncertainties of WT, PV and load demand are modeled in this section.

2.2.1. Probabilistic photovoltaic model

The solar irradiance r approximately obeys the beta distribution for a certain time period [14]. The PV output depends mainly on the amount of solar irradiation, the ambient temperature and the characteristics of the PV modules themselves [40], shown below:

$$f_r(r)=\frac{\Gamma(\lambda_1)+\Gamma(\lambda_2)}{\Gamma(\lambda_1)\Gamma(\lambda_2)}\left(\frac{r}{r_{max}}\right)^{\lambda_1-1}\left(1-\frac{r}{r_{\max}}\right)^{\lambda_2-1} \tag{5}$$

where $\Gamma(\bullet)$ is the gamma function. The PV output P^{PV} is expressed as $P^{PV}=rA^{PV}\eta^{PV}$, where A^{PV} and η^{PV} denote the PV radiation area and the conversion efficiency. The probability density function (PDF) of the PV output is:

$$f_P(P_i^{PV})=\frac{\Gamma(\lambda_1)+\Gamma(\lambda_2)}{\Gamma(\lambda_1)\Gamma(\lambda_2)}\left(\frac{P_i^{PV}}{P_{\max}^{PV}}\right)^{\lambda_1-1}\left(1-\frac{P_i^{PV}}{P_{\max}^{PV}}\right)^{\lambda_2-1} \tag{6}$$

The actual generated power of the PV panel $P_{PV}(t)$ in time slot t, mainly influenced by two factors, the ambient temperature and the solar radiation intensity [40], presented as follows:

$$P_{PV}(t)=\sum_{i=1}^{N_{pv}}P_{rpv}f_{Pv}\left(\frac{R_a(t)}{R_s}\right)\left[1+k\left(T_a(t)-T_s\right)\right] \tag{7}$$

The actual temperature of the PV cells is estimated from the actual solar radiation intensity $R_a(t)$ and the actual ambient temperature, which denotes as $T_a(t)=T_{ae}(t)+0.0256R_a(t)$ [41].

2.2.2. Probabilistic wind turbine model

The output power of the wind turbine varies with the wind speed, the output power of the wind turbine is obtained by the linear interpolation method based on the actual wind speed. The actual power of the wind turbine in time slot t is mainly determined by the cut-in and cut-out wind speed. The PDF of the wind speed is $f_w(v)=(k/c)(v/c)^{k-1}\exp[-(v/c)^k]$, where v, k and c are the actual wind speed, the shape factor and the scale factor. The WT output P^{WT} is described below:

$$P^{WT}=\begin{cases}0, & v<v_{in}, v\geq v_{out}\\ [(v-v_{in})/(v_{rated}-v_{in})]P_{rated}, & v_{in}\leq v\leq v_{rated}\\ P_{rated}, & v_{rated}\leq v\leq v_{out}\end{cases} \tag{8}$$

where v_{rated} and P_{rated} are the rated wind speed and the WT rated power output; v_{in} and v_{out} denote cut-in and cut-out

wind speed. According to (8), the WT output PDF is formulated below, where $h=(v_{rated}/v_{in})-1$:

$$f_W(P_i^{WT})=\begin{cases}0, & P_i^{WT}<0\\ 1\text{-}\exp\{\text{-}[(1+hP_i^{WT}/P_{rated})v_{in}/z]^u\} & \\ +\exp[\text{-}(v_{out}/z)^u], & 0\le P_i^{WT}<P_{rated}\\ 1, & P_i^{WT}\ge P_{rated}\end{cases} \tag{9}$$

$$P_{WT}=\sum_{i=1}^{N_{WT}}P_i^{WT} \tag{10}$$

2.2.3. Probabilistic load model

Load fluctuations are characterized by a widely used normal distribution model, the PDF is described below [42]:

$$f_l\left(P^L\right)=\frac{1}{\sqrt{2\pi}\sigma_L}\exp\left(-\frac{\left(P^L-\mu_L\right)^2}{2\sigma_L^{\,2}}\right) \tag{11}$$

where P^L is the fluctuating load, μ_L and σ_L are the mean and standard deviation of the load.

2.2.4. Equivalent load model

To facilitate the inclusion of multiple random variables, the equivalent load power (EL) is defined as the difference between the total load power and the combined WT, PV, GT and FC output power, P^{EL} denotes the EL power:

$$\begin{aligned}P^{EL}=&P_E+P_{EV}+P_{ELZ}+P_{EC}+P_{EB}\\ &-\left(P_{WT}+P_{PV}+P_{GT}+P_{FC}\right)\end{aligned} \tag{12}$$

2.3. subsystems modeling

2.3.1. Conventional gas turbine power generation

The natural gas consumption and waste heat generated by CGT is calculated [41], where δ is 33.50 MJ/m^3 [43,44]:

$$Q_{gas}=\frac{P_{gt}(t)T(t)}{\beta_1\delta}+\frac{Q_{gb}}{\beta_2\delta} \tag{13}$$

$$Q_{wh} = P_{GT}(t)\frac{1-\beta_1-\varepsilon}{\beta_1} \tag{14}$$

2.3.2. Cooling and heating subsystem

WHBs and ACs are the terminals of waste heat utilization: AC uses waste heat to supply the cooling load and WHBs use waste heat to supply the heat load. The relationship is below:

$$Q_{wh} = \frac{Q_{whb}}{\gamma_{whb}} + \frac{Q_{ac}}{\gamma_{ac}} \tag{15}$$

$$Q_{eb} = \gamma_{eb} H_{eb} \tag{16}$$

The sources of supply of cooling and heating loads are summarized below:

$$Q_C = Q_{ac} + Q_{ec} \tag{17}$$

$$Q_H = Q_{whb} + Q_{gb} + Q_{eb} \tag{18}$$

2.3.3. Hydrogen energy storage subsystem

The hydrogen produced by electrolysis is stored in a hydrogen storage tank under pressure by a compressor. More physical fluid characteristics are referred to the literature [45,46]. The model of the hydrogen storage tank is below:

$$\begin{aligned} V_{hst}(t) &= V_{hst}(t-1) + V_{hst,t}^{in} - V_{hst,t}^{out} \\ &= V_{hst}(t-1) + [P_{sum}(t) - \frac{P_{TE}(t)}{\tau_1}]\tau \end{aligned} \tag{19}$$

2.3.4. PGST operation subsystem

The power-to-gas-to-storage tank (PGST) operation model in the HESS converts the surplus available output of REPG or purchased power during the valley hours into hydrogen, while stored in the hydrogen storage tank to supply FCs cogeneration during the peak hours, which improves the ability to absorb clean energy, reduces the abandonment of the REPG, enables the power-gas-power cycle mode and improves the economic and environmental benefits of the IES[47]. The P2G chemical reaction is $2H_2O \xrightarrow{\text{electrolysis}} 2H_2 + O_2$, PGST contains the P2G and the gas-to-tank process. Equipping HESS in remote isolated parks allows flexible participation in the operation of IES. The energy state in the storage tank is expressed below:

$$S_{GST,t} = S_{GST,t_0} + \sum_{t=1}^{T} \eta_{GST} Q_{GST,t}^{P2G} \tag{20}$$

2.4. Objective function

The rising economic development requires an increase in energy consumption, which accordingly leads to the global environmental pollution [48]. Annual comprehensive cost (ACC) and annual carbon emission (ACE) are used to denote the optimization objective of the economic and environmental performance. First, a single-objective optimization is performed with the objectives of minimizing ACC, minimizing ACE, to obtain the minimum ACC, ACE under single-objective optimization, labeled as ACC_1 and ACE_1. Then, an objective function based on deviation preference is constructed to optimize ACC, ACE simultaneously, labeled as ACC_2 and ACE_2. The weighting coefficient is determined based on the decision-makers' preference. First, decision-makers engaged a decision panel consisting of more than two-thirds of technical and economic experts for a specific project, using a weighted average method, and then determine the weighting coefficients for environmental and economic objectives by means of the expert evaluating method. The objective function has the following advantages: 1) unifying the dimensions of ACC, ACE; 2) optimizing ACC, ACE by weight coefficients simultaneously. The objective function constructed is expressed as follows:

$$\text{Min(deviation satisfaction)} = W_1 \frac{ACC_2 - ACC_1}{ACC_1} + W_2 \frac{ACE_2 - ACE_1}{ACE_1} \tag{21}$$

where W_1, W_2 denote the weight coefficients to indicate the optimization preference. When $\max(W_1, W_2) = W_1$, it places more emphasis on economic performance, and vice versa. In addition, $W_1 + W_2 = 1$.

2.4.1. The objective function of ACC

The annual comprehensive cost (ACC) is one of the important objectives of system configuration optimization. ACC (Eq. (22)) includes major equipment purchase cost (Eq. (23)), O&M(operation and maintenance)cost (Eq.(24)), fuel (natural gas) purchase cost (Eq. (25)), electrolytic water purchase cost (Eq.(26)), carbon tax (Eq.(27)), hydrogen purchase cost (Eq. (28)). Where the carbon tax is composed of a piecewise linear function based on a ladder-type carbon trading mechanism by constructing a piecewise linear function, shown below:

$$ACC = C_{pa} + C_{om} + C_f + C_w + C_{carbontax} + C_{ph} \tag{22}$$

$$C_{pa} = \left(\sum_{i=1}^{n} a_i c_i \right) \frac{k(1+k)^t}{(1+k)^t - 1} \tag{23}$$

$$C_{om} = \sum_{i=1}^{n} a_i c_{iom} \tag{24}$$

$$C_f = Q_{gas} c_{gas} \tag{25}$$

$$C_w = Q_w c_w \tag{26}$$

$$E_{\mathrm{IES},t} = ACE - \mathrm{ACE}_{Quota}$$

$$C_{carbontax} = \begin{cases} T_c E_{\mathrm{IES},t} & E_{\mathrm{IES,t}} < l \\ T_c (1+\alpha)(E_{\mathrm{IES},t} - l) + T_c l & l \le E_{\mathrm{IES,t}} < 2l \\ T_c (1+2\alpha)(E_{\mathrm{IES},t} - 2l) + T_c (2+\alpha) l & 2l \le E_{\mathrm{IES,t}} < 3l \\ T_c (1+3\alpha)(E_{\mathrm{IES},t} - 3l) + T_c (3+3\alpha) l & 3l \le E_{\mathrm{IES,t}} < 4l \\ T_c (1+4\alpha)(E_{\mathrm{IES},t} - 4l) + T_c (4+6\alpha) l & 4l \le E_{\mathrm{IES,t}} < 5l \\ T_c (1+5\alpha)(E_{\mathrm{IES},t} - 5l) + T_c (5+10\alpha) l & 5l \le E_{\mathrm{IES,t}} < 6l \\ T_c (1+6\alpha)(E_{\mathrm{IES},t} - 6l) + T_c (6+15\alpha) l & E_{\mathrm{IES,t}} \ge 6l \end{cases} \tag{27}$$

$$C_{ph} = Q_{ph} \left(c_{hp} + c_{ht} \right) \tag{28}$$

where a_i represents the installed capacity; c_i and c_{iom} represent the unit price and O&M cost; k represents the interest rate of bank loans (4.9%); t indicates the repayment period (20 years); c_{gas} indicates the unit price of natural gas(2.8¥/m^3); c_w indicates the unit price of treated water(4.1¥/m^3) and T_c represents the base price of the carbon tax(20¥/ton) [49]. Q_{ph} denotes the amount of hydrogen purchased. c_{hp} and c_{ht} are the hydrogen production and transportation cost. The hydrogen production cost is about 21.3 ¥/kg [41]. The unit price of a long tube trailer for transportation within 200 km is about 11.03 ¥/kg [41].

2.4.2. The objective function of ACE

Since the energy source of IES is mainly from natural gas, among them, natural gas as a fossil fuel generates CDEs and emits CO_2 through the equipment sources of CGT and GB, ACE is an important indicator of IES regarding environmental performance and the mathematical expression of ACE is calculated below:

$$ACE = Q_{gas}\varphi_1 \tag{29}$$

$$Q_{gas} = \frac{P_{GT}(t)T(t)}{\beta_1\delta} + \frac{Q_{nb}}{\beta_2\delta} \tag{30}$$

where φ_1 (φ_1 =2.01kg［43］) represents CDE (kg/m^3) by burning one cubic meter of natural gas.

2.5. Constraints

The constructed IES contains several constraints, such as equipment, power balance, renewable energy, power supply reliability, site spatial & resource constraints and spinning reserve constraints.

2.5.1. Equipment constraints

(1) Capacity restriction of equipment constraints:

$$UP_i^{min} \le P_i \le UP_i^{max} \tag{31}$$

$$U = \begin{cases} 0, \text{When the unit is shut during slot } t \\ 1, \text{When the unit is on during slot } t \end{cases} \tag{32}$$

where P_i^{min} and P_i^{max} represent the minimum and maximum power.

(2) The start-up and shut-down condition constraint:

$$\begin{cases} \left(U_{t-1} - U_t\right)\left(T_{t-1}^{on} - T^{on}\right) \ge 0 \\ \left(U_t - U_{t-1}\right)\left(T_{t-1}^{off} - T^{off}\right) \ge 0 \end{cases} \tag{33}$$

where T_{t-1}^{on} and T_{t-1}^{off} denote the continuous on/off time of the equipment before the time slot t. The equipment in operation do not remain continuously on and off simultaneously.

(3) Climbing power constraint:

$$\begin{cases} \Delta P_{down} \le P_t - P_{t-1} \le \Delta P_{up} \\ 0 \le P_t \le P_{t,rated} \end{cases} \tag{34}$$

where ΔP_{down} , ΔP_{up} and $P_{t,rated}$ denote the falling power, climbing power and rated power.

2.5.2. Electrical, thermal and cooling balance constraints

Power balance constraint: the generation output of GTs, PVs, WTs and FCs equal to the power of the electric load, ELZs input power and ECs is the input power is below:

$$P_{GT}+P_{PV}+P_{WT}+P_{FC}+P^{EL}=P_{E}+P_{EV}+P_{ELZ}+P_{EC}+P_{EB} \tag{35}$$

where ELZs and FLs do not run at the same working state simultaneously, which divided into two parts: ELZs working and FCs working states, which express as follows:

$$\begin{cases} P_{GT}+P_{PV}+P_{WT}+P_{FC}+P^{EL}=P_{E}+P_{EV}+P_{EC}+P_{EB} \\ P_{GT}+P_{PV}+P_{WT}+P^{EL}=P_{E}+P_{EV}+P_{ELZ}+P_{EC}+P_{EB} \end{cases} \tag{36}$$

where P_E and P_{EV} represent the power demand of the electric load and EVs load; P_{ELZ}, P_{EC}, P_{EB} denotes the input power of ELZ, EC, EB.

2.5.3. Thermal balance constraint

The output thermal power of WHB and GB should satisfy the power required by the thermal load:

$$P_{WHB}+P_{GB}+P_{EB}=P_{HL} \tag{37}$$

where P_{HL} represents the heat load; P_{WHB}, P_{GB} and P_{EB} represent the output power of WHB, GB and EB.

2.5.4. Cooling balance constraint

The output power of ACs and ECs must satisfy the power required by the cooling load:

$$P_{AC}+P_{EC}=P_{CL} \tag{38}$$

where P_{CL}, P_{AC} and P_{EC} represents the cooling load demand, ACs power output and ECs power output.

2.5.5. Hydrogen energy storage system constrains

The operating power of the ELZ must satisfy the following condition:

$$0.05P_{ELZ}^{rated} \le P_{oELZ} \tag{39}$$

where P_{ELZ}^{rated} represents the rated power of ELZ; P_{oELZ} represents the operating power of ELZ and the energy consumption of ELZ to produce one mole of hydrogen is ∂. The equivalent SOC of HSTs should satisfy the upper and lower bound constraints is as follows:

$$SOC_{HST}^{\min} \le SOC_{HST} \le SOC_{HST}^{max} \tag{40}$$

where $SOC_{HST}^{\min}$ is 0 and SOC_{HST}^{max} is 0.9.

2.5.6. Renewable energy constraints

To make full use of the rich renewable energy and reduce the environmental pollution caused by fossil fuels, the REPG installed capacity ratio f_{renew} is not less than its lower boundary $f_{\text{renew,min}}$, where $L_{\max}$ is the annual peak load:

$$f_{\text{renew}} = \frac{N_{\text{WT}} P_{\text{WT}} + N_{PV} P_{\text{PV}}}{L_{\max}} \geq f_{\text{renew,min}} \tag{41}$$

2.5.7. Power supply reliability constraint

When the total output of distributed power supply is not sufficient to meet the load demand, partial load cutting is required. However, the loss of power supply probability (LPSP) should be within the lower and upper limits, the smaller the upper limit value, the higher the reliability of the IES power supply [50]:

$$f_{\text{LPSP,min}} \leq \frac{\sum_{t=1}^{8760} P_{\text{loss}}(t)}{\sum_{t=1}^{8760} \text{load}(t)} \leq f_{\text{LPSP,max}} \tag{42}$$

2.5.8. Site spatial and resources constraints

The available space for PV panels, WTs, HSTs and economic and supplier resources for ELZs and FCs is limited in the IES. Therefore, the number of these types of equipment is expressed:

$$0 \leq N \leq N_{max} \tag{43}$$

where $N = \{N_{PV}, N_{WT}, N_{HST}, N_{ELZ}, N_{FC}\}$ represents the number of PV panels, WTs, HSTs and ELZs, ELZs and FCs; $N_{PV,max}$, $N_{WT,max}$, $N_{HST,max}$, $N_{ELZ,max}$, $N_{FC,max}$ denotes the maximum number.

2.5.9. Spinning reserve constraints

The functions of storage device and grid participating is considered in the provision of reserve services. In the case of no RGs output, the spinning reserve constraint [51] is as below:

$$R_t^{grid} \leq P_{\max}^{e,grid} - \left(P_{e,t}^{EL} + P_{e,t}^{HL} + P_{e,t}^{CL} + P_{e,t}^{GL}\right) \tag{44}$$

$$R_t^{ESD} \leq \min\left\{\eta_{dc}\left(C_t^{ESD} - C_{\min}^{ESD}\right)/\Delta t, P_{dc,\max}^{ESD} - P_{dc,t}^{ESD}\right\} \tag{45}$$

$$P_{rob}\left\{R_t^{grid} + R_t^{ESD} \geq E\left(P_t^{RG}\right) - P_t^{WT} - P_t^{PV}\right\} \geq \alpha \tag{46}$$

where α is considered as a pre-given confidence level.

2.6. Solution approach

Based on the above model, the uncertainty problem is transformed into a deterministic MILP, and BBA is applied to solve it. Our main work is modeling and the algorithm is based on the Cplex solver, which is commonly applicable in the power system industry, and uses existing proven algorithms that are recognized as effective.

2.6.1. Definition of SOT

Sequence operation theory (SOT) is used as a tool to deal with uncertainty based on sequence convolution in the field of digital signal processing [52]. The probability distributions of random variables are represented by probability sequences, and the new sequences is obtained from operations between sequences.

Definition 1: A discrete sequence $a(i)$ is called a probability sequence when its length N_a satisfies the following definition:

$$\sum_{i=0}^{N_a} a(i) = 1, a(i) \geq 0,\ i = 1, 2, ..., N_a \tag{47}$$

Definition 2: The expectation of the given probabilistic sequence $a(i)$ with the length N_a , defined below:

$$E(a) = \sum_{i=0}^{N_i} \left[ia(i) \right] = \sum_{i=1}^{N_i} \left[ia(i) \right] \tag{48}$$

2.6.2. Serialization of random variables

The discretized step transformation (DST) is a mathematical tool that has been used to handle multiple uncertainties based on SOT [14]. The PV and WT outputs of REPG are random variables in time slot t . The PDF of PV and WT is discretized into pieces to obtain probability sequences $a(i_{at})$ and $b(i_{bt})$. The probabilistic sequence length of P_{PV} is shown as:

$$N_{at} = \left\lceil P_{max,t}^{PV} / q \right\rceil \tag{49}$$

where $\lceil \bullet \rceil$ is the ceiling function; $P_{max,t}^{PV}$ denotes the maximum output power of PV unit in time slot t ; q is the discrete step size; the PV unit has a total number of $N_{at}+1$ states. Thus, the output of state m_a is $m_a q (0 \leq m_a \leq N_{at})$, and the corresponding probability is $a(m_a)$. According to SOT, the probabilistic sequence $a(i_{at})$ of the PV output [53] is:

$$a\left(i_{at}\right)=\begin{cases}\int_{0}^{q/2} f_p\left(P^{PV}\right)dP^{PV}, & i_{at}=0\\ \int_{i_{at}q-q/2}^{i_{at}q+q/2} f_p\left(P^{PV}\right)dP^{PV}, & 0<i_{at}<N_{at}\\ \int_{i_{at}q-q/2}^{i_{at}q} f_p\left(P^{PV}\right)dP^{PV}, & i_{at}=N_{at}\end{cases} \tag{50}$$

According to the above discretization method, the probabilistic sequence $b\left(i_{bt}\right)$ of WT outputs is calculated. Based on both, the probabilistic sequence of the joint outputs $c\left(i_{ct}\right)$ is derived:

$$\begin{aligned} c\left(i_{ct}\right) &= a\left(i_{at}\right)\oplus b\left(i_{bt}\right)\\ &= \sum_{i_{at}+i_{bt}=i_{ct}} a\left(i_{at}\right)b\left(i_{bt}\right),\ i_{ct}=0,1,...,N_{at}+N_{bt}\end{aligned} \tag{51}$$

The expected value of renewable energy, $E\left(P_t^{RG}\right)$, is gained as follows:

$$\begin{aligned} E\left(P_t^{RG}\right) &= E\left(P_t^{PV}\right)+E\left(P_t^{WT}\right)\\ &= \sum_{m_{at}=0}^{N_{at}} m_{at}qa\left(m_{at}\right)+\sum_{m_{bt}=0}^{N_{bt}} m_{bt}qb\left(m_{bt}\right)\end{aligned} \tag{52}$$

Similarly, the probability sequence of fluctuating load $d\left(i_{dt}\right)$ and equivalent load $e\left(i_{et}\right)$ is given below:

$$\begin{aligned} e\left(i_{et}\right) &= d\left(i_{dt}\right)\ominus c\left(i_{ct}\right)\\ &= \begin{cases}\sum_{i_{dt}-i_{ct}=i_{et}} d\left(i_{dt}\right)c\left(i_{ct}\right),\ i_{et}=1,...,N_{et}\\ \sum_{i_{dt}\le i_{ct}} d\left(i_{dt}\right)c\left(i_{ct}\right),\ i_{et}=0\end{cases}\end{aligned} \tag{53}$$

2.6.3. Deterministic transformation of chance constraint

To convert the chance constraint **(46)** into its deterministic equivalence class, let: $Z=P_t^{WT}+P_t^{PV}$, the distribution of the variable Z is below:

$$F_Z\left(z\right)=\int_{-\infty}^{z}\left[\int_{-\infty}^{\infty} f_w\left(z-y\right)f_p\left(y\right)dy\right]dz \tag{54}$$

However, the form of the PDF_S listed above is too complicated to handle, so the transformation from chance constraint to its deterministic class is accomplished by SOT to handle the probability distribution of the variable Z. The probability sequence of the joint REPG and EL power is shown in Table 2 and Table 3, given below:

$$c\left(m_{ct}\right)=\sum_{m_{at}+m_{bt}=m_{ct}} a\left(i_{at}\right)b\left(m_{bt}\right),m_{ct}=0,1,2,...,N_{at}+N_{bt} \tag{55}$$

The Eq.**(46)** is not solved directly because it is a chance constraint. Therefore, a new binary variable ω_m is introduced below:

$$\omega_m = \begin{cases} 1, R_t^{grid} + R_t^{ESD} \geq E\left(P_t^{RG}\right) - m_{ct} q, m_{ct} = 0,1,...,N_{ct} \\ 0, \text{otherwise} \end{cases} \tag{56}$$

The chance constraint is then simply expressed as follows:

$$\sum_{m_{ct}=0}^{N_{at}+N_{bt}} \omega_m c\left(m_{ct}\right) \geq \alpha \tag{57}$$

where Eq. (57) shows that the spinning reserve capacity of the MG satisfies the condition that the required confidence level is greater than or equal to α for all possible output values corresponding to the EL in period t. Therefore, Eq. (57) is equivalent to Eq. **(46)** , which is converted into a deterministic equivalent form. The original model cannot be solved directly and efficiently because it contains uncertainties in the probability distribution of the new energy generation. It needs to be transformed into a solvable MILP by three steps, including transforming the joint probability distribution of wind power generation and PV power generation, deterministic transformation of the chance constraint, and linearization, so that the deterministic equivalent form is represented as a solvable MILP. The solution process of the proposed DST approach is shown in Figure 5.

2.6.4. Analytical framework

Figure 6 summarizes the analytical framework. All simulations were performed on a PC platform with Radeon Graphics CPUs (3GHz) and 16 GB RAM. After the above mathematical conversion steps, the obtained optimal configuration model was transformed into a MILP. The simulation is based on the YALMIP language environment, which runs the code on the MATLAB platform and calls CPLEX to solve the model. In this simulation, the branch-and-bound algorithm (BBA) under CPLEX 12.6 was used to solve the problem.

3. Simulation

The parameters of various types of equipment in the IES are from literature [41,54–56] in this simulation. Furthermore, the number of EVs $N = 1000$, the proportion of EVOs affected by electricity price $\eta = 0.2$. We simulated an industrial park in three-north regions of China. This simulation was conducted with a discrete step size of 2.5 kW, a confidence level of 90%, and load fluctuations of 10%. As shown in

Figure 7 and

Figure 8, the data were obtained for 8760 hours in a year of wind and PV power output. The natural wind-PV-hydrogen-gas-EV in the IES was designed to supply the various energy loads, including EV load demand. Figure 9 shows the distribution of load data for six types of loads including EVs on a typical day.

3.1. Confidence level on reserve capacity

By selecting different confidence levels, the corresponding spinning reserve capacity was obtained, shown in Figure 10. As we can see, compared to other confidence levels, the 100% confidence level behaves differently at peaks and suddenly reach a higher value, which indicates that fully reliable operation requires the supply of a very high reserve capacity and is not very cost effective. The required spinning reserve capacity gradually increases as the confidence level increases accordingly, which inevitably leads to higher operating costs for the CIES, indicating an increase in the operational reliability of the CIES. Meanwhile, this increases the operating cost. Therefore, an appropriate confidence level is necessary to be chosen to trade off the reliability and cost effectiveness.

3.2. Analysis of discrete steps

The discretized step transformation (DST) method is introduced to solve CCP. When using DST, step size q affects spinning reserve capacity, when it is small, the computational accuracy is higher, but it inevitably leads to the problem of too large probability sequences, resulting in a sharp increase in computation time. In contrast, a larger step size saves computational time, but leads to the generated sequence not fully reflecting the actual probability distribution. The choice of step size was analyzed and the results are shown in Figure 11.

3.3. Optimal configuration results

The optimization results are outlined in Table 4.The investment and procurement of the 11 pieces of equipment, shown in detail for the cost and investment structure under the original optimization model in Figure 12 and Figure 13. The equipment procurement cost of HESS accounts for about two-thirds of the total cost, while the procurement cost of REPG including WTs and PVs, CCHP including GTs, ACs and WHBs accounts for more than 30%， HESS subsystem accounting for the largest share of equipment procurement costs, as HSTs and FCs account for the major procurement costs of HESS. GTs account for nearly 80% of the CCHP system. The procurement cost of CCHP is mainly from GTs, while the procurement cost of HESS is mainly derived from HSTs and FCs. The breakthrough in reducing the equipment procurement cost is primarily focused on FCs, HSTs and GTs. In reality, HESS costs including HSTs and FCs is excessively expensive, which accounts for a large proportion of the

equipment procurement cost, HSTs, FCs and GTs are the equipment that should be prioritized for cost reduction. The cost structure of HESS needs to be optimized. In addition, the procurement cost of hydrogen is too high, and more hydrogen should be produced by using electrolysis in HESS through excess electricity from REPG to meet the park's demand. However, as technological advancements and the emergence of the scale effect, the investment value will be highlighted. The typical daily load supply of various types of equipment output is shown in Figure 14. Overall, the coordinated optimization of the IES has put the energy supply and demand in a relatively stable state.

4. Further discussion and analysis

4.1. Sensitivity analysis

Table 5 summarizes the optimization results. Figure 15 shows the performance in terms of cost and CDEs. CDER in this IES results in an increase in cost, which is mainly due to the increase in FCs. When the optimization preference is changed from ($W_1 = 0.6, W_2 = 0.4$) to ($W_1 = 0.3, W_2 = 0.7$), the lower cost increase results in significant CDER. While the preference shifts from ($W_1 = 0.3, W_2 = 0.7$) to ($W_1 = 0.1, W_2 = 0.9$), only limited CDER is achieved at the higher growth cost. Moreover, when the preference shifts from ($W_1 = 0.6, W_2 = 0.4$) to ($W_1 = 0.9, W_2 = 0.1$), the preference changes have little effect on CDEs and cost fluctuations, while when the preference shifts from ($W_1 = 0.9, W_2 = 0.1$) to ($W_1 = 1, W_2 = 0$), the lower cost decrease produces significant CDEs, implying that the cost-effective performance of this optimization shift is unworthy. As a result, pursuing either environmental or cost objectives is inappropriate in this case, the decision-makers' optimal optimization preference range is concentrated between ($W_1 = 0.1, W_2 = 0.9$) and ($W_1 = 0.6, W_2 = 0.4$).

4.2. Comparative analysis

4.2.1. Annual carbon emission comparison of CDS and IES

Power generation is mainly derived from REPG and natural gas in this IES. The former is a zero-carbon emission, while the latter generates CDEs [57], When the CDER level of the IES is evaluated, the results show that there is a significant advantage in CDER when compared to the Conventional Distribution System (CDS). The comparative optimization scenario setting is shown in Table 6.

In terms of CDEs, the original optimization scenario shows a significantly higher CDER than the conventional distribution scenario. The directly generated E_{ACE2} in this IES are only 20.05% of the CDS when the ACE from hydrogen is excluded. Options for hydrogen sourcing include fossil fuel-based hydrogen production (grey

hydrogen), fossil fuel-based hydrogen production combined with carbon capture, utilization and storage (CCUS, blue hydrogen), and renewable hydrogen (green hydrogen). Assuming that hydrogen in CDS is produced using coal gasification technology and the hydrogen purchased in the IES is produced by natural gas reforming with 56% carbon capture technology (CCT). When comparing CDEs from hydrogen, the advantages of IES are clear, ACE in this IES accounts for only 24.98% of the CDS. Overall, ACE in this IES accounts for only 22.59% of the CDS. The specific details are shown in Table 7 and Figure 16.

4.2.2. Electric vehicle group comparison of IES and non-IES

A comparative calculation between the two situations in terms of ACE and total annual charging cost was made to analyze the operation level of different EVGs in the IES and non-IES regions. The assumptions include: (i) EVG charging cost includes both electric charging cost and charging service fee，and the charging service fee is 0.8 ¥/kWh, which is incurred due to investment in charging piles, operation and maintenance; (ii) The charging cost outside the radiation area of EVG is composed of TOU price and the charge service fee, using electricity from thermal power generation, while the charging cost of EVG in the IES is based on the reference value of no EV charging demand and the increased ACC as charging cost after considering a certain scale of EVs, plus the same charging service fee, the above calculation is seen as EVG charging cost. (iii) CDEs in the IES are composed of CDEs produced directly by the IES and CDEs produced from the purchased hydrogen by natural gas reforming with 56% CCT. (iv) TOU prices are divided into valley hours at 0.307 ¥/kWh from 22:00 to 06:00 and peak hours at 0.617 ¥/kWh from 06:00 to 22:00.

A comparison of charging costs and carbon emissions associated with the different EVG between IES and non-IES is shown in Figure 17. In general, the charging cost and ACEs in the IES and non-IES follow a relatively linear trend as the EVG size increases. Charging costs in the IES are lower than charging in the non-IES, with a relatively small difference between different EVG, while charging in the IES results in much lower CDEs than those in the non-IES. As a result, charging in the IES has not only tremendous environmental value but also a certain economic value.

4.3. Scenario analysis

Site constraints, natural gas prices and the number of EVs are all essential factors that affect the optimal value of the IES. The optimization results obtained for these three scenarios are summarized in Table 8 and Table 9. The analysis of the scenario with no site constraints or supplier resource constraints for the park compares the

optimization results without resource constraints such as WTs, PVs, HSTs, ELZs and FCs, shown in Table 8; the natural gas price and the number of EVs are shown in Table 9. Conclusions is drawn with W_1=0.3, W_2=0.7 as the benchmark: when there are no spatial and resource limitation of PV panels, HST, or ELZ, the number of those types of equipment increases, ACC increases, but ACE decreases. While the resource constraints of WTs and FCs have almost no effect on the optimal value. When there are no spatial and resource constraints, ACC increases and ACE decreases, but relatively slower. When the natural gas price rises, ACC rises and ACE falls, while the number of EVs rises, both ACC and ACE rise. The former is because an increase in natural gas cost raises the overall cost, but the expensive natural gas cost causes customers to switch to renewable energy sources, resulting in CDER. The latter is because the increased use of EVs will directly increase the use of electricity and gas consumption, leading to increases in ACC and ACE. However, the growth of CDEs is relatively slow, while the use of EVs indirectly reduces the use of gasoline vehicles, which is beneficial to CDER.

4.4. Carbon tax policy analysis

Site constraints, natural gas prices and the number of EVs are all essential factors that affect the optimal value of

Carbon tax policy primarily employs a tax on CDEs. In the new electricity market, carbon emissions are a freely tradable commodity, and there is a baseline in China to determine non-reimbursable carbon emission quotas. The current Chinese carbon tax base price is 20 ¥/ton [49], while the natural gas base price is 2.80 ¥/m^3 . When natural gas price changes, ACC will increase due to an increase in the base carbon tax price or natural gas price, while ACE will decrease due to an increase in the carbon tax base price or natural gas price. When the carbon tax is lower than the base price, not only will CDER be unaffected, but it will also increase ACC. These results strongly suggest that current carbon tax policies are ineffective in providing incentives to reduce ACE. In comparison, the natural gas price is more sensitive, a 100-fold increase in carbon tax price would be required to equal the CDER achieved by a 4-fold increase in natural gas price. The current carbon tax policy is ineffective in reducing the CDEs of the IES, and the current carbon tax threshold in China is too low compared to other countries. Under the current carbon tax policy, an increase in natural gas price is more conducive to achieving CDER since the increased cost of natural gas fuel will cause users to substitute with REPG, reducing CDEs. As seen in Figure 18, different decision preferences result in significant differences in the optimal value of CDEs. The best CDER is obtained when the base carbon tax price is increased to 10 to 50 times while the natural gas price is increased by 2 to 3 times, with the same focus on economic and environmental objectives (w1=0.5, w2=0.5). An increase in carbon taxes alone has no effect when

there is more emphasis on economic goals. Consequently, a good carbon tax policy should consider not only the carbon tax adjustment, but also the change in natural gas price.

5. Conclusions and future work

A natural wind-PV-hydrogen-gas-EV IES is constructed, a decision preference is introduced to characterize the decision maker's preferences, and an objective optimization model based on preference deviation is established. The following conclusions is drawn:

1) Multiple uncertainties are considered by SOT and CCP, the spinning reserve provided by the storage device and the external grid is established. By setting an appropriate confidence level, the capacity configuration achieves a trade-off between economy and reliability; 2) Sensitivity analysis is used to derive the results of the capacity configuration for various decision preferences, the optimal range was found between (W_1=0.1, W_2=0.9) and (W_1=0.6, W_2=0.4); 3) CDEs of IES are only one-fifth of those in CDS and the CDER effect is noticeable. Moreover, EV charging cost in the IES is relatively lower, while the CDER effect is an order of magnitude better than that of non-IES; 4) The inclusion of EV in the IES shows benefits in terms of economic and environmental performance.

In further research, hydrogen fuel cell vehicles will be used as the demand side of FCs supply, while the discharge behavior of EVs in V2G model will be introduced to deepen the capacity configuration research. We will also consider the realistic constraints of IES, such as the physical thermal characteristics of fluids [58] in hydrogen energy storage.

Declaration of Competing Interest

The authors declare that there is no conflict of interests regarding the publication of this paper.

References

1. Davis, S. J., Lewis, N. S., Shaner, M., etal. “Net-zero emissions energy systems”, *Science*, **360**(6396), p. eaas9793 (2018).
2. Ufa, R. A., Malkova, Y. Y., Gusev, A. L., etal. “Algorithm for optimal pairing of res and hydrogen energy storage systems”, *International Journal of Hydrogen Energy*, **46**(68), pp. 33659–33669 (2021).
3. Chu, S. and Majumdar, A., “Opportunities and challenges for a sustainable energy future”, *Nature*, **488**(7411), pp. 294–303 (2012).
4. Stouffer, R. J. and Manabe, S., “Assessing temperature pattern projections made in 1989”, *Nature Clim Change*, **7**(3), pp. 163–165 (2017).
5. Hanley, E. S., Deane, J. P., and Gallachóir, B. Ó. “The role of hydrogen in low carbon energy futures–A review of existing perspectives”, *Renewable and Sustainable Energy Reviews*, **82**, pp. 3027–3045 (2018).

6. Wang, Y., Wang, X., Yu, H., etal. “Optimal design of integrated energy system considering economics, autonomy and carbon emissions”, *Journal of Cleaner Production*, **225**, pp. 563–578 (2019).
7. Crespi, E., Colbertaldo, P., Guandalini, G., etal. “Design of hybrid power-to-power systems for continuous clean PV-based energy supply”, *International Journal of Hydrogen Energy*, **46**(26), pp. 13691–13708 (2021).
8. Xu, C., Ke, Y., Li, Y., etal. “Data-driven configuration optimization of an off-grid wind/PV/hydrogen system based on modified NSGA-II and CRITIC-TOPSIS”, *Energy Conversion and Management*, **215**, p. 112892 (2020).
9. Zhang, F., Zhao, P., Niu, M., etal. “The survey of key technologies in hydrogen energy storage”, *International Journal of Hydrogen Energy*, **41**(33), pp. 14535–14552 (2016).
10. Syri, S., Lehtilä, A., Ekholm, T., etal. “Global energy and emissions scenarios for effective climate change mitigation—Deterministic and stochastic scenarios with the TIAM model”, *International Journal of Greenhouse Gas Control*, **2**(2), pp. 274–285 (2008).
11. Pal, A., Bhattacharya, A., and Chakraborty, A. K., “Placement of electric vehicle charging station and solar dg in distribution system considering uncertainties”, *Scientia Iranica* (2021).
12. Wang, J., Dong, F., Ma, Z., etal. “Multi-objective optimization with thermodynamic analysis of an integrated energy system based on biomass and solar energies”, *Journal of Cleaner Production*, **324**, p. 129257 (2021).
13. Akram, F., Asghar, F., Majeed, M. A., etal. “Techno-economic optimization analysis of stand-alone renewable energy system for remote areas”, *Sustainable Energy Technologies and Assessments*, **38**, p. 100673 (2020).
14. Li, Y., Han, M., Yang, Z. etal. “Coordinating flexible demand response and renewable uncertainties for scheduling of community integrated energy systems with an electric vehicle charging station: A bi-level approach”, *IEEE Transactions on Sustainable Energy*, **12**(4), pp. 2321–2331 (2021).
15. Lan, T., Jermsittiparsert, K., T. Alrashood, S., etal. “An Advanced Machine Learning Based Energy Management of Renewable Microgrids Considering Hybrid Electric Vehicles’ Charging Demand”, *Energies*, **14**(3), p. 569 (2021).
16. Li, X., Sun, B., Ju, W., etal. “Capacity Configuration Model of Biogas-based Integrated Energy System”, *2021 IEEE 4th International Electrical and Energy Conference (CIEEC)*, pp. 1–6 (2021).
17. Zhang, L., Gao, Y., Zhu, H., etal. “Bi-level stochastic real-time pricing model in multi-energy generation system: A reinforcement learning approach”, *Energy*, **239**, p. 121926 (2022).
18. Elmaadawy, K., Kotb, K. M., Elkadeem, M. R., etal. “Optimal sizing and techno-enviro-economic feasibility assessment of large-scale reverse osmosis desalination powered with hybrid renewable energy sources”, *Energy Conversion and Management*, **224**, p. 113377 (2020).
19. Rezaei, M., Dampage, U., Das, B. K., etal. “Investigating the Impact of Economic Uncertainty on Optimal Sizing of Grid-Independent Hybrid Renewable Energy Systems”, *Processes*, **9**(8), p. 1468 (2021).
20. Li, B., Li, X., and Su, Q., “A system and game strategy for the isolated island electric-gas deeply coupled energy network”, *Applied Energy*, **306**, p. 118013 (2022).
21. Hadidian-Moghaddam, M. J., Arabi-Nowdeh, S., Bigdeli, M., etal. “A multi-objective optimal sizing and siting of distributed generation using ant lion optimization technique”, *Ain Shams Engineering Journal*, **9**(4), pp. 2101–2109 (2018).
22. Lu, S., Li, Y., and Xia, H., “Study on the configuration and operation optimization of CCHP coupling multiple energy system”, *Energy Conversion and Management*, **177**, pp. 773–791 (2018).
23. Yamano, S., Nakaya, T., Ikegami, T., etal. “Optimization modeling of mixed gas engine types with different maintenance spans and costs: Case study OF CCHP to evaluate optimal gas engine operations and combination of the types”, *Energy*, **222**, p. 119823 (2021).

24. Yang, D., Wang, M., Yang, R., etal. "Optimal dispatching of an energy system with integrated compressed air energy storage and demand response", *Energy*, **234**, p. 121232 (2021).
25. Jiang, Y., Kang, L., and Liu, Y., "The coordinated optimal design of a PV-battery system with multiple types of PV arrays and batteries: A case study of power smoothing", *Journal of Cleaner Production*, **310**, p. 127436 (2021).
26. Lin, H., Yang, C., and Xu, X., "A new optimization model of CCHP system based on genetic algorithm", *Sustainable Cities and Society*, **52**, p. 101811 (2020).
27. Nazari, M. H., Hosseinian, S. H., Azad Farsani, E., etal. "An incentive-based policy on minimization of GHG emissions and loss using adaptive group search multi-objective optimization algorithm", *Scientia Iranica*, **29**(1), pp. 230–246 (2022).
28. Esmaeilion, F., Ahmadi, A., and Dashti, R., "Exergy-economic-environment optimization of the waste-to-energy power plant using multi-objective particle-swarm optimization (MOPSO)", *Scientia Iranica*, **28**(5), pp. 2733–2750 (2021).
29. Qari, H., Khosrogorji, S., and Torkaman, H., "Optimal sizing of hybrid WT/PV/diesel generator/battery system using MINLP method for a region in Kerman", *Scientia Iranica*, **27**(6), pp. 3066–3074 (2020).
30. Zhong, J., Li, Y., Cao, Y., etal. "Stochastic optimization of integrated energy system considering network dynamic characteristics and psychological preference", *Journal of Cleaner Production*, **275**, p. 122992 (2020).
31. Prasanthi, A., Shareef, H., Asna, M., etal. "Optimization of hybrid energy systems and adaptive energy management for hybrid electric vehicles", *Energy Conversion and Management*, **243**, p. 114357 (2021).
32. Liu, Z., Guo, J., Wu, D., etal. "Two-phase collaborative optimization and operation strategy for a new distributed energy system that combines multi-energy storage for a nearly zero energy community", *Energy Conversion and Management*, **230**, p. 113800 (2021).
33. Wang, Y., Wang, Y., Huang, Y., etal. "Planning and operation method of the regional integrated energy system considering economy and environment", *Energy*, **171**, pp. 731–750 (2019).
34. Xiang, Y., Cai, H., Gu, C., etal. "Cost-benefit analysis of integrated energy system planning considering demand response", *Energy*, **192**, p. 116632 (2020).
35. Wang, Y., Ma, Y., Song, F., etal. "Economic and efficient multi-objective operation optimization of integrated energy system considering electro-thermal demand response", *Energy*, **205**, p. 118022 (2020).
36. Yuan, G., Gao, Y., and Ye, B., "Optimal dispatching strategy and real-time pricing for multi-regional integrated energy systems based on demand response", *Renewable Energy*, **179**, pp. 1424–1446 (2021).
37. Kaheh, Z., Baradaran Kazemzadeh, R. B., and Sheikh-El-Eslami, M. K., "A solution based on fuzzy max-min approach to the bi-level programming model of energy and exiramp procurement in day-ahead market", *Scientia Iranica*, **27**(2), pp. 846–861 (2020).
38. Qian, K., Zhou, C., Allan, M., etal. "Modeling of Load Demand Due to EV Battery Charging in Distribution Systems", *IEEE Transactions on Power Systems*, **26**(2), pp. 802–810 (2011).
39. Tian, L., Shi, S., and Jia, Z., "A statistical model for charging power demand of electric vehicles", *Power System Technology*, **34**(11), pp. 126–130 (2010).
40. Laudani, A., Fulginei, F. R., and Salvini, A., "Identification of the one-diode model for photovoltaic modules from datasheet values", *Solar energy*, **108**, pp. 432–446 (2014).
41. Zhou, J., Wu, Y., Zhong, Z., etal. "Modeling and configuration optimization of the natural gas-wind-photovoltaic-hydrogen integrated energy system: A novel deviation satisfaction strategy", *Energy Conversion and Management*, **243**, p. 114340 (2021).
42. Li, Y., Wang, R., and Yang, Z., "Optimal scheduling of isolated microgrid with an electric vehicle battery swapping station in multi-stakeholder scenarios: A bi-level programming approach via real-time pricing", *IEEE Transactions on Sustainable Energy*, **13**(1), pp. 159–169 (2018).
43. Zhou, J., Wu, Y., Wu, C., etal. "A hybrid fuzzy multi-criteria decision-making approach for performance

analysis and evaluation of park-level integrated energy system", *Energy Conversion and Management*, **201**, p. 112134 (2019).
44. Zhou, J., Wu, Y., Dong, H., etal. "Proposal and comprehensive analysis of gas-wind-photovoltaic-hydrogen integrated energy system considering multi-participant interest preference", *Journal of Cleaner Production*, **265**, p. 121679 (2020).
45. Oveissi, S., Toghraie, D., and Eftekhari, S. A., "Longitudinal vibration and stability analysis of carbon nanotubes conveying viscous fluid", *Physica E: Low-dimensional Systems and Nanostructures*, **83**, pp. 275–283 (2016).
46. Toghraie, D., "Numerical thermal analysis of water's boiling heat transfer based on a turbulent jet impingement on heated surface", *Physica E: Low-Dimensional Systems and Nanostructures*, **84**, pp. 454–465 (2016).
47. Ju, L., Zhao, R., Tan, Q., etal. "A multi-objective robust scheduling model and solution algorithm for a novel virtual power plant connected with power-to-gas and gas storage tank considering uncertainty and demand response", *Applied Energy*, **250**, pp. 1336–1355 (2019).
48. Rashit, O., Slushash, A., Dauren, O., etal. "Integrated system for the use of solar energy in the animal farm", *Scientia Iranica*, **24**(6), pp. 3213–3222 (2017).
49. Zhao, X., Wu, L., and Zhou, Y., "How to achieve incentive regulation under renewable portfolio standards and carbon tax policy? A China's power market perspective", *Energy Policy*, **143**, p. 111576 (2020).
50. Sadeghi, D., "Optimal sizing of hybrid renewable energy systems in presence of electric vehicles using multi-objective particle swarm optimization", *Energy*, **209**, p. 118471 (2020).
51. Li, Y., Wang, C., Li, G., etal. "Optimal scheduling of integrated demand response-enabled integrated energy systems with uncertain renewable generations: A Stackelberg game approach", *Energy Conversion and Management*, **235**, p. 113996 (2021).
52. Wang, Y., Zhang, N., Chen, Q., etal. "Dependent Discrete Convolution Based Probabilistic Load Flow for the Active Distribution System", *IEEE Transactions on Sustainable Energy*, **8**(3), pp. 1000–1009 (2017).
53. Li, Y., Wang, C., Li, G., etal. "Improving operational flexibility of integrated energy system with uncertain renewable generations considering thermal inertia of buildings", *Energy Conversion and Management*, **207**, p. 112526 (2020).
54. Duman, A. C. and Güler, Ö., "Techno-economic analysis of off-grid PV/wind/fuel cell hybrid system combinations with a comparison of regularly and seasonally occupied households", *Sustainable Cities and Society*, **42**, pp. 107–126 (2018).
55. Khiareddine, A., Ben Salah, C., Rekioua, D., etal. "Sizing methodology for hybrid photovoltaic /wind/ hydrogen/battery integrated to energy management strategy for pumping system", *Energy*, **153**, pp. 743–762 (2018).
56. Liu, Z., Chen, Y., Zhuo, R., etal. "Energy storage capacity optimization for autonomy microgrid considering CHP and EV scheduling", *Applied Energy*, **210**, pp. 1113–1125 (2018).
57. Ye, B., Gao, Y., and Yuan, G., "Renewable energy investment study for electric power enterprise based on a time period with expected supply", *Enterprise Information Systems*, pp. 1–26 (2021).
58. Dabiri, S., Khodabandeh, E., Poorfar, A. K., etal. "Parametric investigation of thermal characteristic in trapezoidal cavity receiver for a linear Fresnel solar collector concentrator", *Energy*, **153**, pp. 17–26 (2018).

Table 1 summarizes some of the recent studies on capacity configuration optimization in IES.

Literature	Year	Main components of IES	Optimization objectives	Optimization tools

[12]	2021	Biomass + solar energies	ATCSR+CDERR+PESR	NSGA- II
[13]	2020	PV/Wind/Diesel/ Battery	Economic, environmental and reliable power supply	HOMER Pro + cyclic charging algorithm
[14]	2021	CIES with an EVCS in multi-stakeholder scenarios	Upper level: the CIES net operating cost; Lower-level: the EVCS net operating cost	SOT with CCP, MILP+CPLEX
[15]	2021	Renewable microgrids	The total operation cost	A machine learning based approach based on dragonfly
[16]	2021	A biogas-based IES	Annual total cost, annual carbon emissions and exergy efficiency	Augmented ε-constraint method to obtain the Pareto curve
[17]	2022	Thermal power plant + WT/PV Plant	Social welfare	Reinforcement learning
[18]	2020	PV/WT/diesel/battery/inverter system	Net present cost, renewable fraction, cost of energy and CO_2 emission	Homer Pro
[19]	2021	Grid-independent hybrid renewable-based systems	Techno-economic-environmental and reliability	Homer Pro
[20]	2022	IES with a deep coupling of power-gas network	Total income of IES+ energy-saving +environmental protection	Game theory + PSO
[21]	2018	A distribution system	Purchased energy cost + reliability + DGs' application cost + DS losses + voltage deviation	Ant lion optimizer
[22]	2018	CCHP coupled multi-energy system	Annual operating cost	Sequence control +sequential quadratic programming + feedback correction mechanism
[23]	2021	CCHP with gas engines	Operation plan of CCHP +maintenance plan of the gas engines	The load balance of each piece of equipment+ the elapsed time axis to optimize actual maintenance activities
[24]	2021	Compressed air energy storage and sliding time window	The total cost	PDF of the risk variable
[25]	2021	A PV-battery system with multi-type PV arrays and multi-type batteries	The total cost	The smoothing scenario
[26]	2020	A CCHP system	Primary energy saving (PES)+ LC cost reduction (LCCR)+ CDER+ Comprehensive evaluation index (CEI)	GA
[27]	2022	In distribution networks	Loss and emission reduction	Group Search Optimizer with Adaptive Covariance matrix and Chaotic search (MGSOACC)
[28]	2021	In a waste-to-energy power plant	The total exergy efficiency of the cycle + fuel, exergy destruction, equipment, and environment	MOPSO

[29]	2020	In a hybrid system comprising WT/PV/diesel generator/battery	Annual cost (investment + maintenance + fuel consumption of diesel generator)	MINLP and GAMS
[30]	2020	IES stochastic optimization considering the network dynamic characteristics and psychological preference	Comprehensive cost (thermal power unit + gas source output+ penalty + investment+ maintenance)	Auto-regressive and moving average (ARMA) time series
[31]	2021	Hybrid EVs comprising ultracapacitor (UC) and fuel cell (FC)	Initial cost, weight, running cost and cost associated with source degradation.	Improved BOA
[32]	2021	A distributed energy system that combines multi-energy storage considering 3 types of energy storage and EVs load	The annual cost savings rate; the primary energy savings rate	A two-phase collaborative optimization method
[33]	2019	In a regional integrated energy system	Energy and environmental cost +achieve the optimal operation scheme	Two-stage optimization with NSGA-II and MILP
[34]	2020	An optimal planning model on the grid-connected IES considering PBDR and IBDR	The total annual cost	MILP
[35]	2020	An electro-thermal IES with a DR mechanism considering electric load and thermal load	Economic benefits and comprehensive energy efficiency	NSGA-II
[36]	2021	Multiple RIESs with energy production, storage, conversion configurations and various loads	The upper level is the profits of the supplier, the lower level is the RIESs' welfare.	The RTP algorithm based on IDR
[37]	2020	In the day-ahead market	The upper level is the profit, the lower level is energy and spinning reserve procurement cost	A fuzzy max-min approach through fuzzy utility functions

Table 2 The probabilistic sequence of joint renewable energy.

Power (MW)	0	q	...	$m_c q$	...	$N_{ct} q$
Probability	$c(0)$	$c(1)$	...	$c(m_c)$	...	$c(N_{ct})$

Table 3 The probabilistic sequence of EL power.

Power (MW)	0	q	...	$m_c q$	...	$N_{ct} q$
Probability	$e(0)$	$e(1)$	...	$e(m_c)$	...	$e(N_{ct})$

Figure 1 Schematic of the proposed natural wind-photovoltaic-hydrogen-gas-EV IES

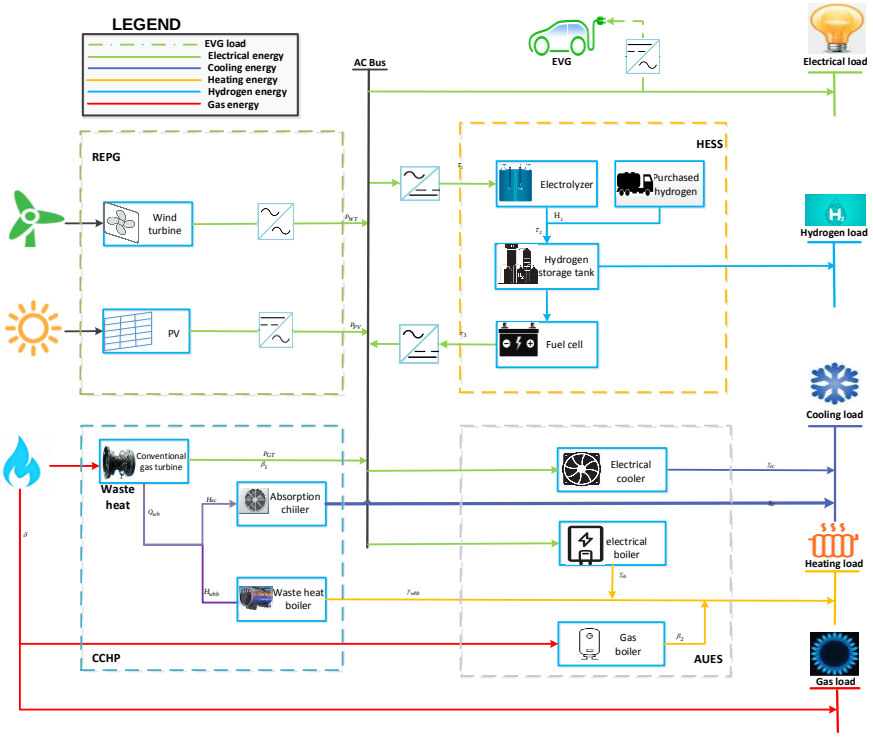

Figure 2 Stochastic charging demand flow diagram for EVs obtained using MC simulation

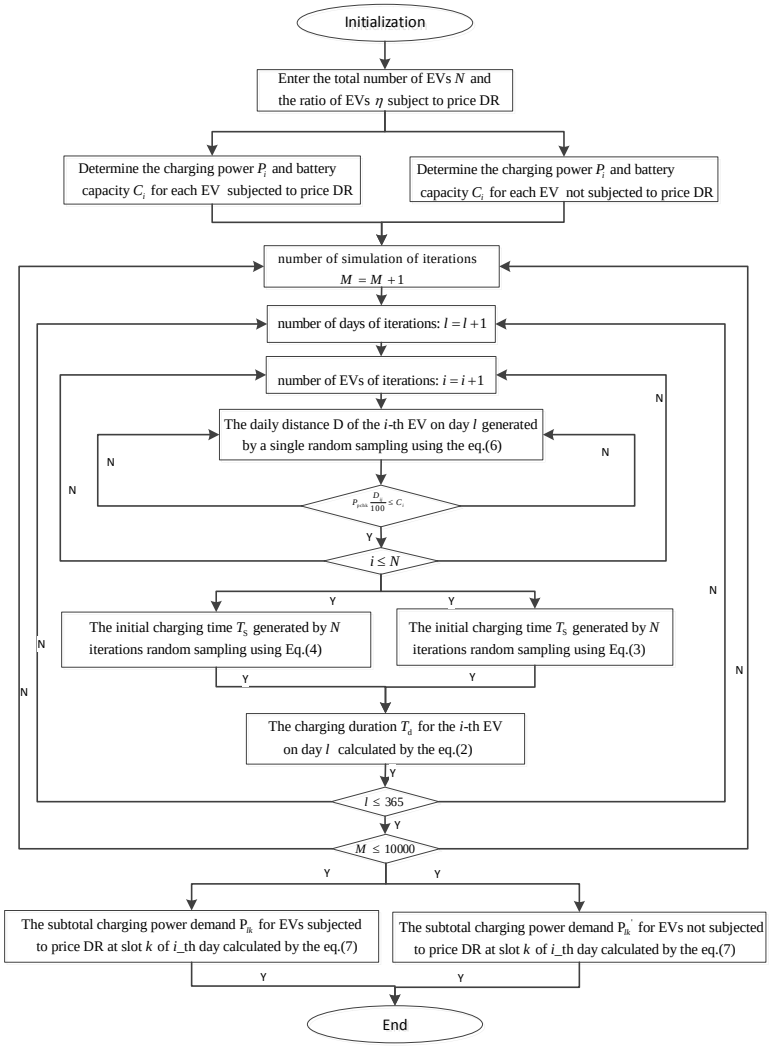

Figure 3 Total daily charging load of EVs including two types of EVOs.

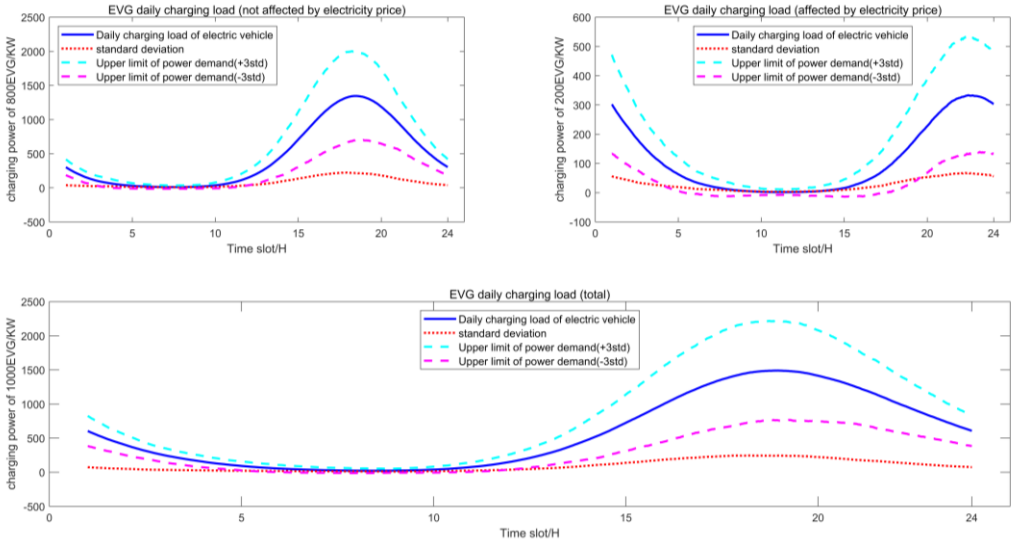

Figure 4 Sensitivity analysis of EV charging load using MC simulation

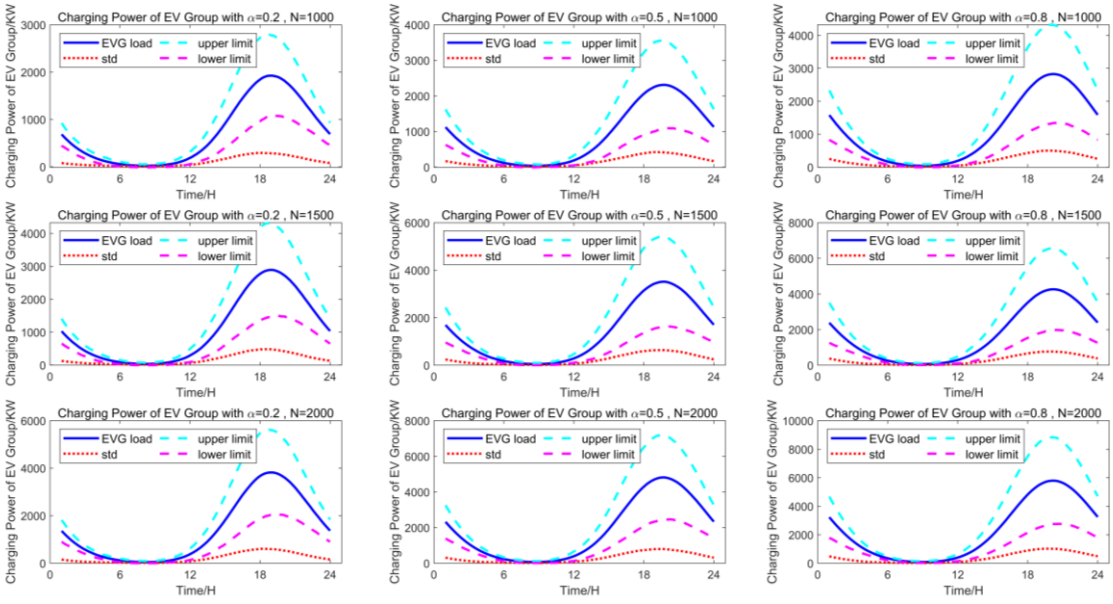

Figure 5 Flow chart of the proposed solution steps

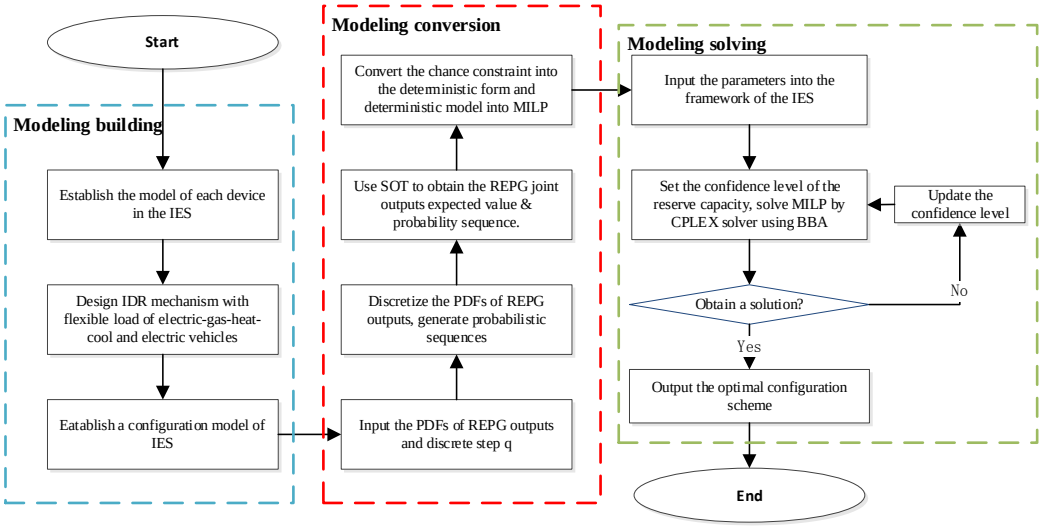

Figure 6 Proposed analytical framework for IES configuration optimization

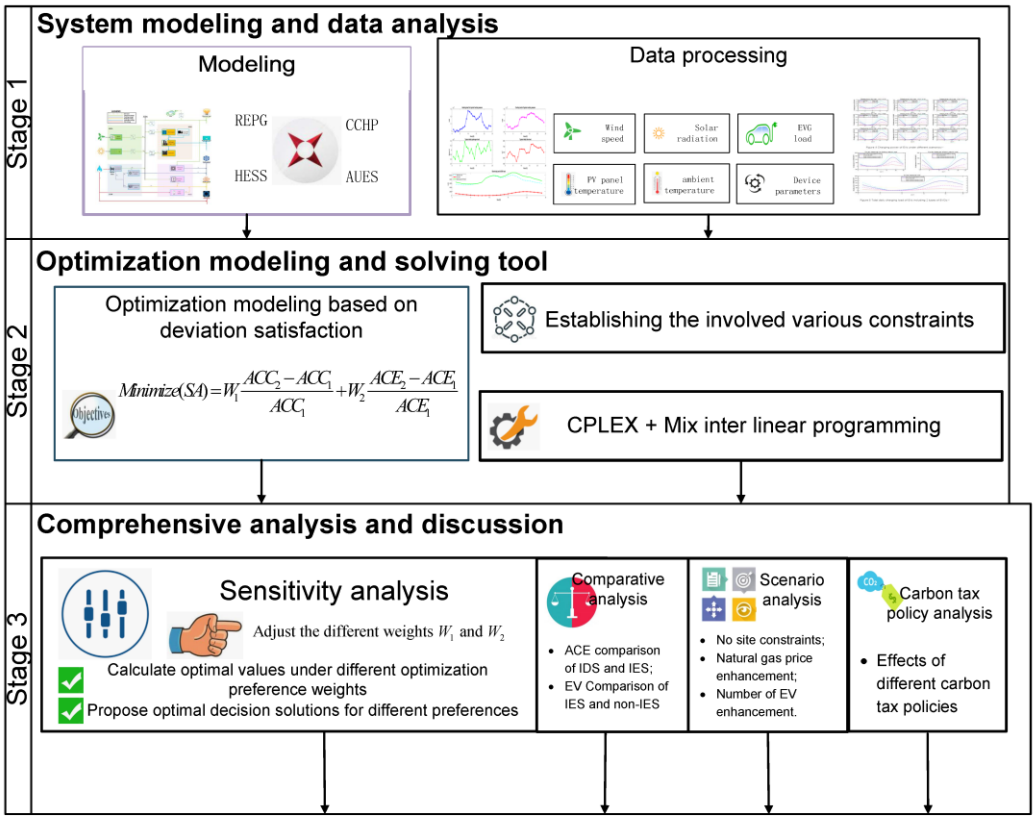

Figure 7 Annual temperature data and output data of the PV panel.

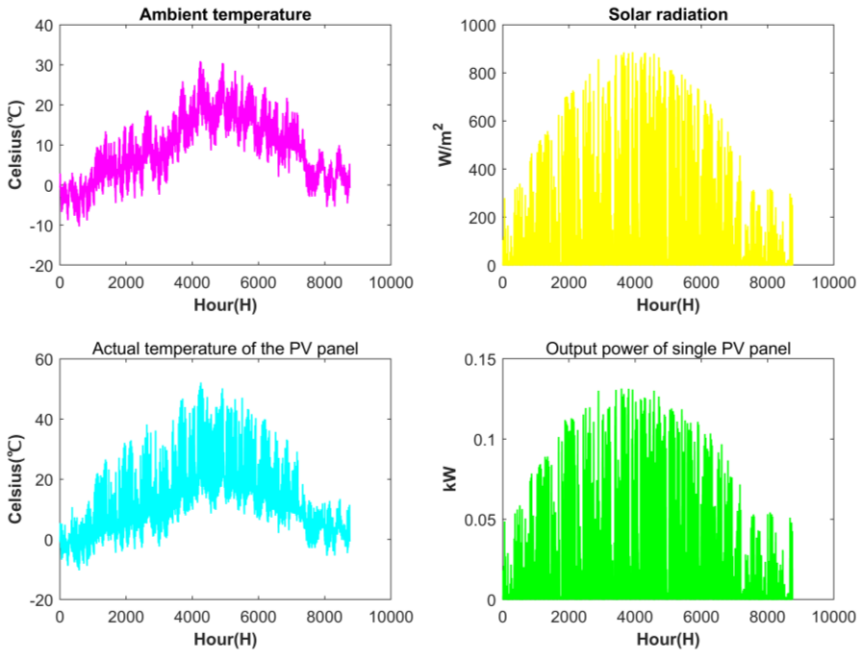

Figure 8 Annual temperature data and output data of the wind turbine.

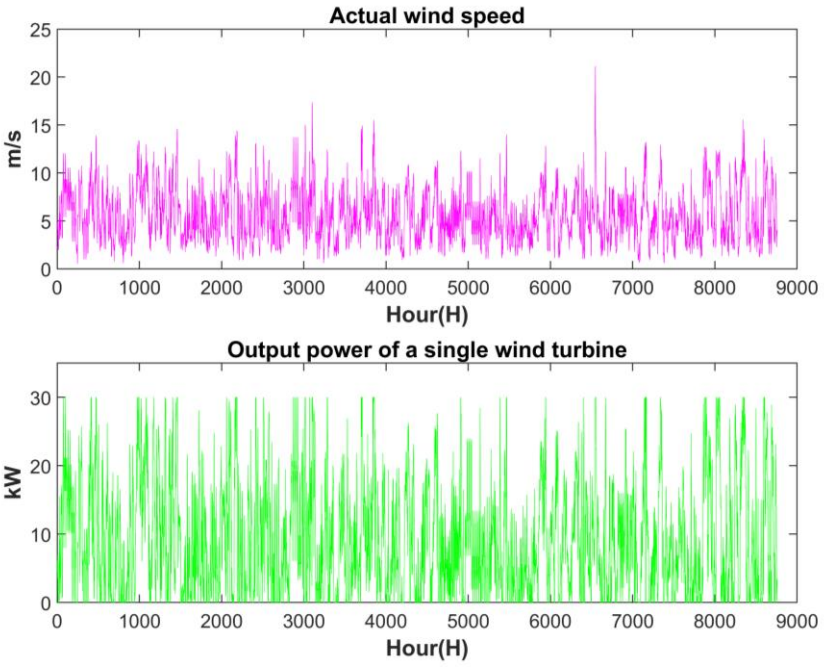

Figure 9 The distribution of heating, cooling, hydrogen loads and electricity & EVG.

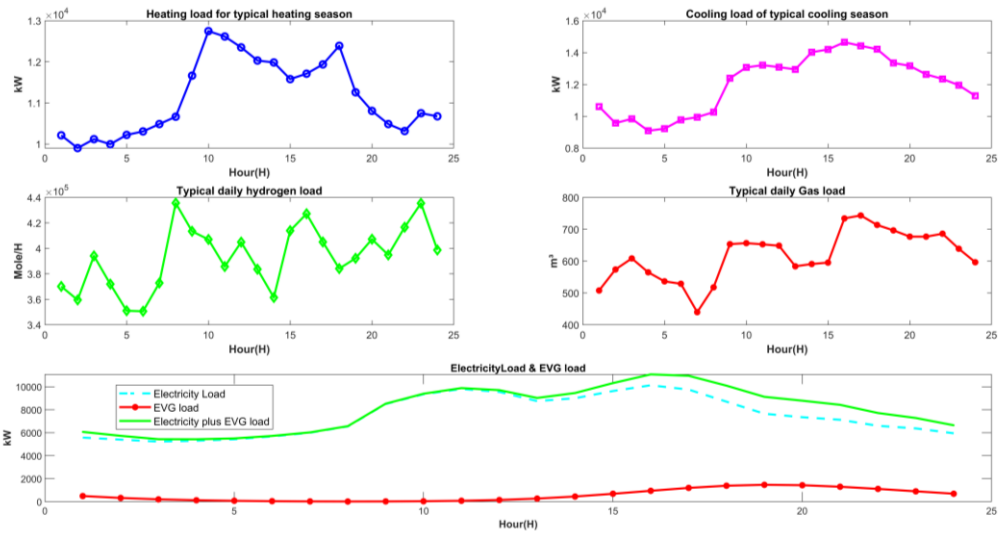

Figure 10 Spinning reserve capacities under different confidence levels.

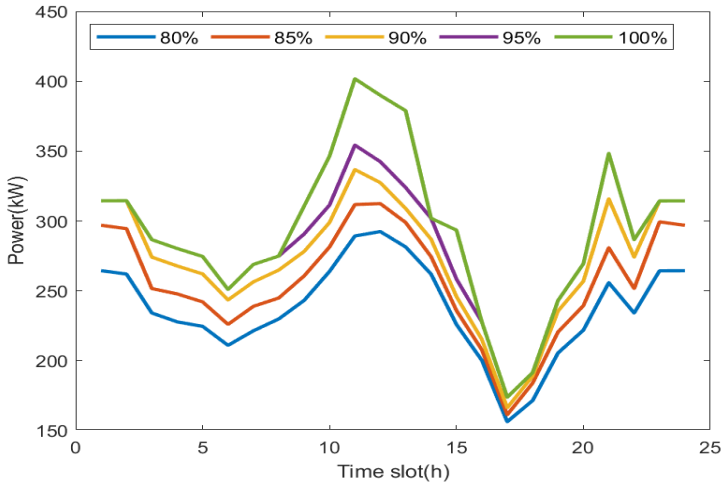

Figure 11 Effects of different discrete steps on the optimal results.

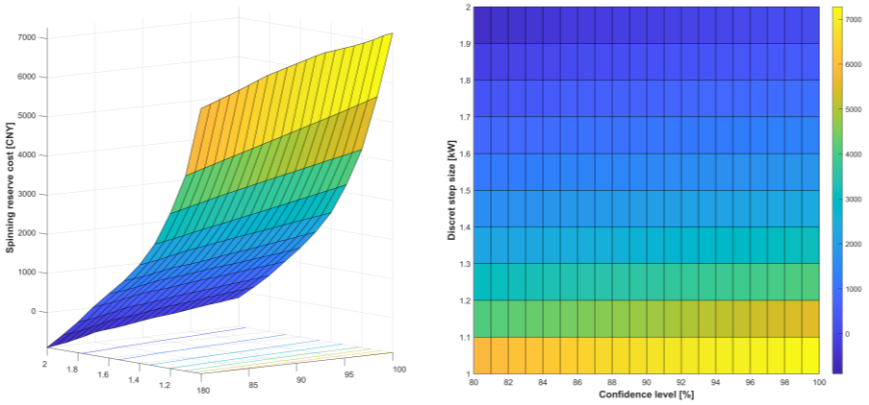

Table 4 The optimal result of the capacity configuration of the original setting (W1=0.3, W2=0.7)

Variable	Configuration result	Variable	Configuration result
a_{GT} (kW)	52	a_{ELZ} (kW)	5
a_{WHB} (kW)	0	a_{HST} (kW)	1600
a_{AC} (kW)	15479	a_{FC} (kW)	88
a_{GB} (kW)	0	$C_{ACC1}(10^8¥)$	2.822
a_{EC} (kW)	10210	E_{ACE1} (10^7 kg)	2.147
a_{EB} (kW)	19121	$C_{ACC2}(10^8¥)$	3.141
a_{PV} (kW)	9000	E_{ACE2} (10^7 kg)	2.403
a_{WT} (kW)	532	SA	0.118

Figure 12 The proportion cost of the main equipment and ACC.

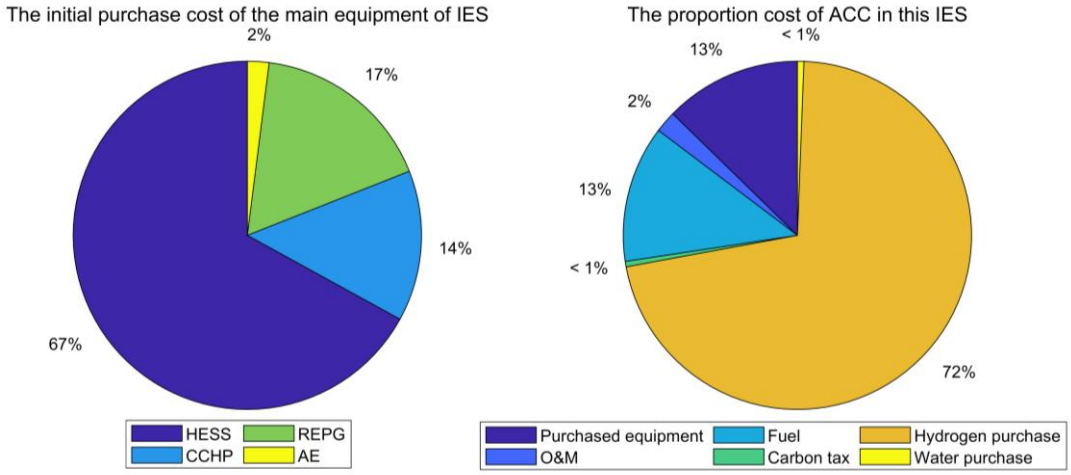

Figure 13 The proportion cost of purchased equipment.

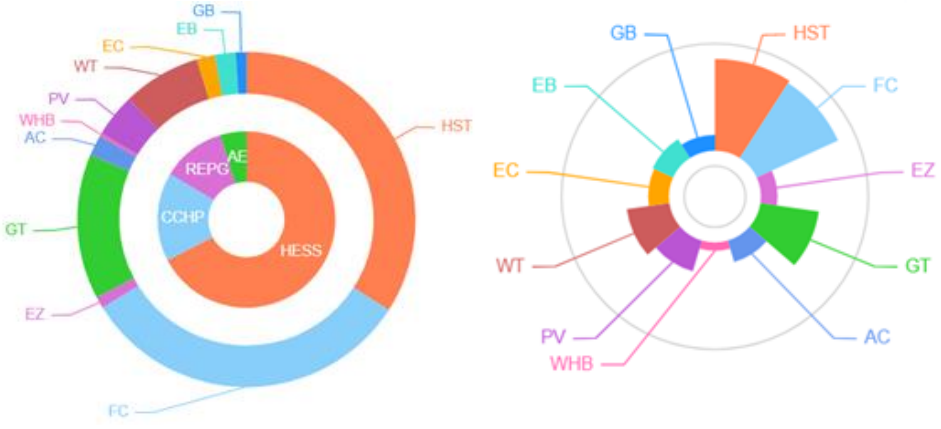

Table 5 The configuration results under different optimization preferences

(W_1,W_2)	(0,1)	(0.1,0.9)	(0.2,0.8)	(0.3,0.7)	(0.4,0.6)	(0.5,0.5)	(0.6,0.4)	(0.7,0.3)	(0.8,0.2)	(0.9,0.1)	(1,0)
a_{GT} (kW)	62	61	50	52	55	58	62	62	62	62	63
a_{WHB} (kW)	1	17906	0	0	17906	2227	17906	3854	3854	3854	4240
a_{AC} (kW)	18539	19392	15137	15479	16489	19392	18443	18568	18568	19392	19066
a_{GB} (kW)	0	19121	0	0	19121	198	125	0	699	34	0
a_{EC} (kW)	19540	21973	10257	10210	21973	9595	9511	9511	9511	9511	4605
a_{EB} (kW)	19122	19121	19121	19121	19121	18924	18919	18924	18422	18528	16888
a_{PV} (kW)	9000	9000	9000	9000	9000	0	0	0	0	0	0
a_{WT} (kW)	532	532	532	532	532	532	511	511	511	511	117
a_{ELZ} (kW)	5	5	5	5	5	5	0	0	0	0	5
a_{HST} (kW)	1600	1600	1600	1600	1600	1600	1432	1432	1432	1432	1428

a_{FC} (kW)	400	247	130	88	58	30	0	0	0	0	0
$C_{ACC1}(10^8¥)$	2.822	2.822	2.822	2.822	2.822	2.822	2.822	2.822	2.822	2.822	2.822
E_{ACE1} (10^7 kg)	2.147	2.147	2.147	2.147	2.147	2.147	2.147	2.147	2.147	2.147	2.147
$C_{ACC2}(10^8¥)$	4.004	3.578	3.258	3.141	3.066	2.947	2.831	2.829	2.829	2.830	2.823
E_{ACE2} (10^7 kg)	2.149	2.309	2.351	2.403	2.469	2.523	2.602	2.602	2.603	2.603	2.876
SA	0.001	0.095	0.107	0.118	0.125	0.110	0.087	0.065	0.045	0.024	0.000
T_{run} (s)	32.81	49.09	49.07	44.73	54.05	70.03	67.98	61.94	67.87	71.55	74.30

Figure 14 Typical daily load supply of various types of equipment output.

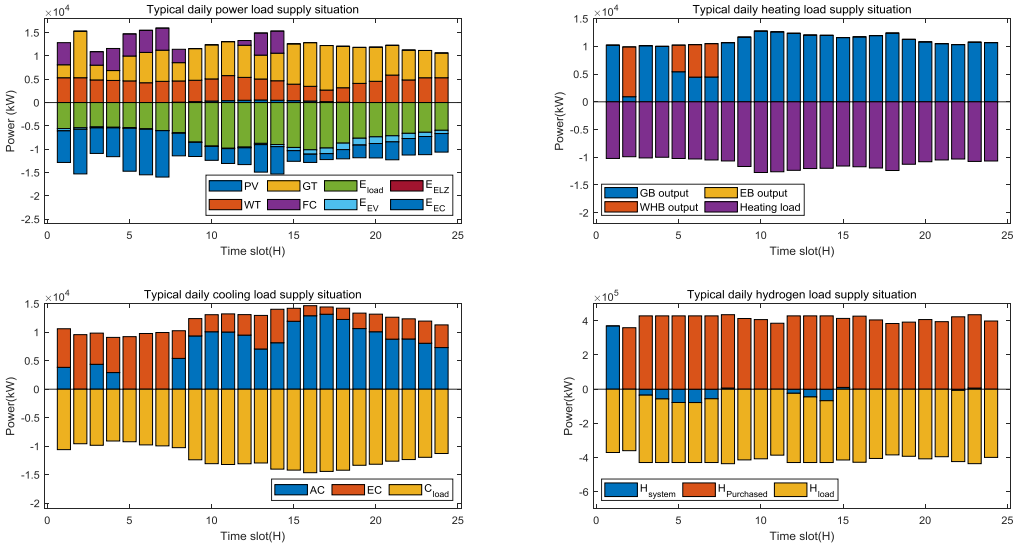

Figure 15 The cost-effectiveness of different optimization preferences.

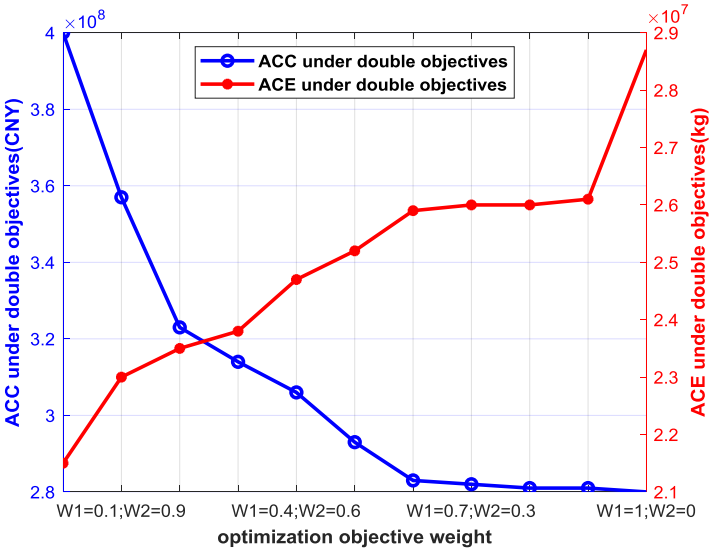

Table 6 comparative optimization scenario description setting

Scenario	CDS	IES
Characteristics	Coal-fired thermal power + GB+EC	W_1=0.3, W_2=0.7, N=1000

Table 7 Comparison results of CDEs between CDS and IES

CDS		IES	
Load Type	CDEs/t	Load Type	CDEs/t
Electricity by Thermal Power	23,642.47		
Heat load by GB	7,039.27	E_{ACE2} by gas supply	24,694.90
Cold load by EC	92,513.38		
Coal gasification to hydrogen	130,902.02	Purchased hydrogen by natural gas(56%CCT)	32,693.79
		Hydrogen from electrolysis via REPG	0.00
Total	254,097.13	Total	57,388.69

Figure 16 The proportion of CDEs between CDS and IES.

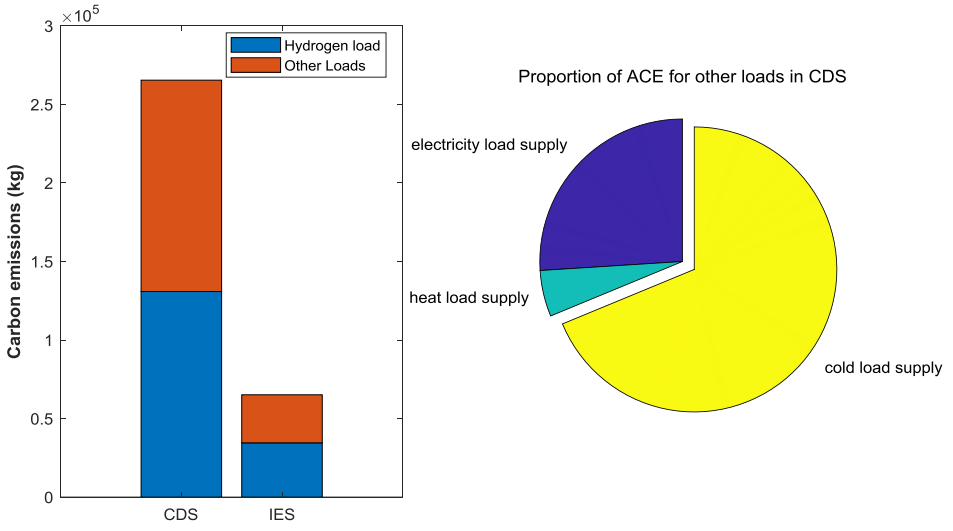

Figure 17 Charging comparison of different EVG between IES and non-IES.

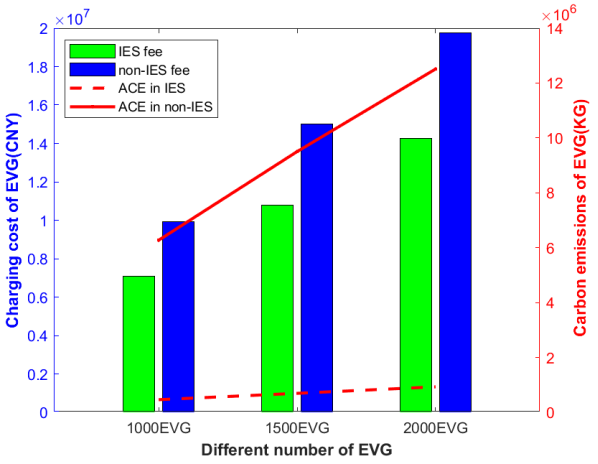

Table 8 Results of capacity optimization configuration in various scenarios

Variables	W_1=0.3, W_2=0.7							
	Original scenario	No resources	No PV/WT	No PV	No WT	No HST	No ELZ	No FC
a_{GT} (kW)	52	10	51	51	52	16	51	52
a_{WHB} (kW)	0	0	0	0	0	17906	19121	4626
a_{AC} (kW)	15479	2926	15394	15394	15479	4654	15342	15400
a_{GB} (kW)	0	0	0	0	0	0	0	0
a_{EC} (kW)	10210	21635	15874	15874	10210	21231	12103	10093
a_{EB} (kW)	19121	19121	19121	19121	19121	19121	19121	19121
a_{PV} (kW)	9000	0	129293	129293	9000	9000	9000	9000
a_{WT} (kW)	532	511	532	532	532	532	800	532
a_{ELZ} (kW)	5	0	5	5	5	5	70	5
a_{HST} (kW)	1600	2531	1600	1600	1600	2483	1600	1600
a_{FC} (kW)	88	450	109	109	88	400	94	86
C_{ACC1}(10^8¥)	2.822	2.814	2.822	2.822	2.822	2.822	2.814	2.822
E_{ACE1} (10^7 kg)	2.147	1.112	1.966	1.966	2.147	1.147	2.025	2.147
C_{ACC2}(10^8¥)	3.141	4.689	3.550	3.550	3.141	4.597	3.395	3.122
E_{ACE2} (10^7 kg)	2.403	1.128	2.189	2.189	2.403	1.155	2.116	2.429
SA	0.118	0.210	0.157	0.157	0.118	0.193	0.093	0.124
T_{run} (s)	44.73	71.14	68.75	68.45	79.13	64.86	57.51	63.70

Table 9 Results of capacity optimization configuration in various scenarios

Variables	W_1=0.3, W_2=0.7							
	Original scenario	Natural gas price increased 4 times	Natural gas price increased 10 times	The number of EVs increased 1.5 times	The number of EVs increased 2 times	The number of EVs increased 5 times	The number of EVs increased 10 times	The number of EVs increased 15 times
a_{GT} (kW)	52	52	61	52	54	60	70	101

a_{WHB} (kW)	0	6422	17906	17906	169	5344	8221	18584
a_{AC} (kW)	15479	14818	19392	19667	15984	17955	21147	21973
a_{GB} (kW)	0	0	19121	0	0	7027	0	0
a_{EC} (kW)	10210	11653	21973	11058	9727	8761	9070	9463
a_{EB} (kW)	19121	19121	19121	19121	19121	19121	19121	19121
a_{PV} (kW)	9000	9000	9000	9000	9000	9000	9000	9000
a_{WT} (kW)	532	532	532	535	537	554	581	608
a_{ELZ} (kW)	5	5	5	5	5	5	5	5
a_{HST} (kW)	1600	1600	1600	1600	1600	1600	1600	1600
a_{FC} (kW)	88	119	218	88	86	87	110	143
$C_{ACC1}(10^8¥)$	2.822	3.916	5.976	2.828	2.835	2.882	3.001	3.368
E_{ACE1} (10^7 kg)	2.147	2.147	2.147	2.170	2.193	2.335	2.633	3.068
$C_{ACC2}(10^8¥)$	3.141	4.221	6.414	3.158	3.184	3.273	3.344	3.562
E_{ACE2} (10^7 kg)	2.403	2.361	2.318	2.419	2.392	2.470	2.842	3.258
SA	0.118	0.093	0.078	0.116	0.100	0.081	0.090	0.061
T_{run} (s)	44.73	72.29	77.33	49.07	55.29	51.48	45.89	35.67

Figure 18 ACE of the effects under different carbon tax and gas price.

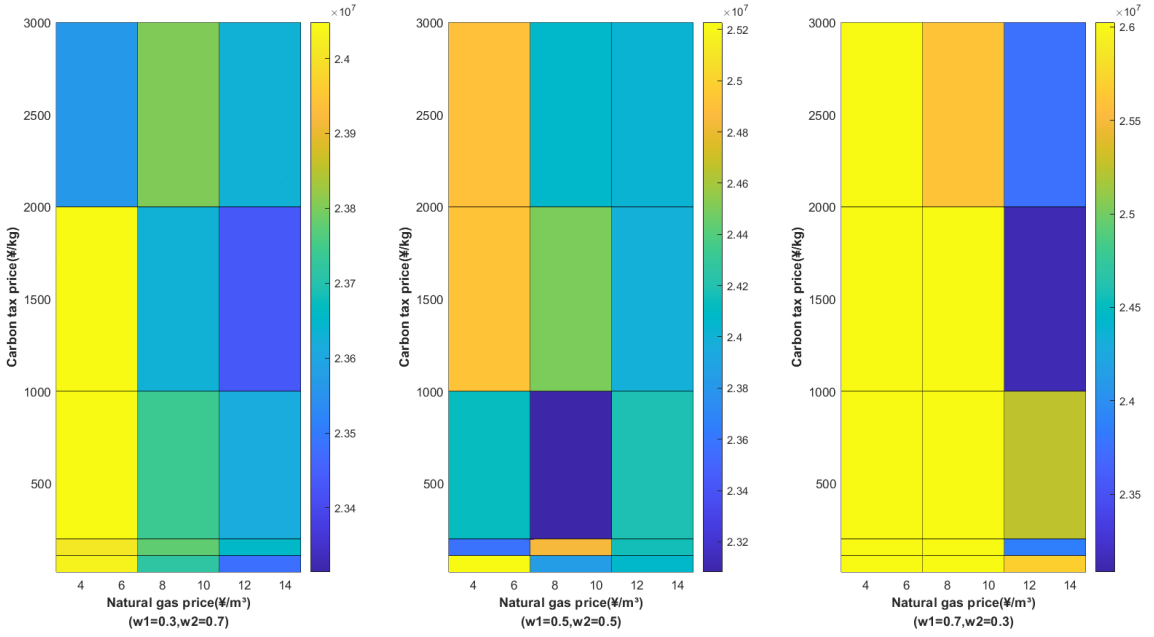

Biographies

Gang Zhu was born in China. He received his master's degree in engineering management from University of Shanghai for Science and Technology in 2019. Currently, he is a PhD candidate in the School of Management at University of Shanghai for Science and Technology. He won the first prize in the paper posting competition at the 5th Chinese Systems Science Conference, and his research interests include integrated energy system optimization and real-time pricing of smart grid.

Yan Gao was born in China. He received his Ph.D. degree from Dalian University of Technology in 1996. Currently, he serve as chair professor at School of Management, University of Shanghai for Science and Technology

. His research focuses on demand-side management and real-time pricing for the smart grid, as well as non-smooth optimization. He has published 300 journal papers and has authored two books.

Hao Sun was born in China. He received his PhD degree in Management Science and Engineering from University of Shanghai for Science and Technology in 2022. Currently, he is working as a postdoctoral fellow at Shandong University. He has published more than ten papers. His research interests include green supply chain, game theory, emergency management and environmental governance.